FINAL REPORT

FOR

EXPERIMENTS A17 (OGO 1) AND B17 (OGO 3)

(16 FEB 1962 - 30 JUN 1968)

CONTRACT NO. NAS 5-2131

Prepared by

Principal Investigator: R. A. Helliwell
Research Physicist: J. J. Angerami

of

The Radioscience Laboratory
Stanford Electronics Laboratories
Stanford University
Stanford, California 94305

for

GODDARD SPACE FLIGHT CENTER
GREENBELT, MARYLAND

RADIOSCIENCE LABORATORY

STANFORD ELECTRONICS LABORATORIES

STANFORD UNIVERSITY · STANFORD, CALIFORNIA

FINAL REPORT

FOR

EXPERIMENTS A17 (OGO 1) AND B17 (OGO 3)

(16 FEB 1962 - 30 JUN 1968)

CONTRACT NO. NAS 5-2131

GODDARD SPACE FLIGHT CENTER

Contracting Officer: John Tominovich
Technical Monitor: E. P. Mercanti

Prepared by

Principal Investigator: R. A. Helliwell
Research Physicist: J. J. Angerami

of

The Radioscience Laboratory
Stanford Electronics Laboratories
Stanford University
Stanford, California 94305

Project Manager: Wilfred E. Scull

for

GODDARD SPACE FLIGHT CENTER
GREENBELT, MARYLAND

LIST OF CONTENTS

LIST OF CONTENTS (cont.)

I. INTRODUCTION

This report summarizes the main results of the research on data from the Stanford University/Stanford Research Institute VLF experiments flown on OGO 1 (A 17) and OGO 3 (B 17). The work has been supported by the National Aeronautics and Space Administration under contract NAS 5-2131.

Chapter 2 briefly describes the orbits and attitudes of both satellites, and presents the main features of the VLF experiments A 17 and B 17. The calibration curves of the corresponding receivers are given in Appendix B.

Chapter 3 outlines the experiment's purposes, and Chapter 4 gives a concise account of the results obtained to date in each of several topics. Specific references are made to the illustrated abstracts of Appendix A. A list of publications acknowledging contract NAS 5-2131 is also given.

II. BACKGROUND

A. SATELLITE ORBIT AND ATTITUDE

OGO 1 was launched on 4 September 1964 and the antenna of experiment A 17 was deployed at 2326Z on 8 September. Its eccentric orbit, with inclination of 31^{o} and period of 63 hours, 59.5 minutes, covered the altitude range 282 to 149,360 km (Table 1). Since the period is nearly 2-2/3 days, successive perigees occur at geographic locations displaced approximately 120 degrees to the east, the same regions being therefore sampled every three orbits. Although intended to be three-axis stabilized, OGO 1 had a spin with period of approximately 12 seconds around an axis within 7 degrees of the z-axis. A more detailed description of the OGO-1 satellite is presented in the IG Bulletin of the National Academy of Sciences [1965].

OGO 3 was launched on 7 June 1966 in an eccentric orbit. The antenna of experiment B 17 was deployed at 0420Z on 15 June. At that time the orbit covered an altitude range of 497 to 121,924 km, with an inclination of 31^{o} and period of 48 hours, 32 minutes (Table 1). Since this period is close to 2 days, successive perigees occur at geographic locations displaced only 10 degrees to the west, and approximately the same region is sampled every two days. OGO 3 was three-axis stabilized, with the +z-axis pointing to the earth and x-axis normal to the sun line, until about 1800Z on 23 July 1966. After 27 July the satellite was spun around the z-axis, with a period of 95 seconds.

For a comprehensive description of the Orbiting Geophysical Observatory missions the report by Ludwig [1965] should be consulted.

Table 1. Orbit parameters of OGO 1 and OGO 3 at antenna deployment.

	launch	Exp 17 antenna deployment	altitude (km)		period	inclination	apogee		
			apogee	perigee			latitude	local time	change in local time (min/orbit)
OGO 1	4 Sep 64	8 Sep 64; 2326Z	149,360	282	63h 59.5min	31°	22°	2112	-10
OGO 3	7 Jun 66	15 Jun 66; 0420Z	121,924	497	48h 32.2min	31°	21°	2106	-8

B. DESCRIPTION OF EXPERIMENTS A 17 AND B 17

The Stanford University/Stanford Research Institute VLF experiments aboard OGO 1 (A 17) and OGO 3 (B 17) consist of an antenna and pre-amplifier(s) at the end of a long boom, and five receivers (four in OGO 1) located in the main body. Figure 24 in Appendix B is a block diagram of the experiment flown on OGO 3. With the two modifications discussed below, it also represents the experiment aboard OGO 1.

The antenna is a loop with 2.9m diameter and 7.6cm diameter cross section, located at the end of the +y, 20-foot boom. The plane of the antenna is normal to the z-axis and therefore horizontal in the stabilized mode, and nearly fixed in space after the satellites were spun.

The package in EP-5 (top left of Figure 24) indicates that the OGO-3 antenna can be connected through the matching transformer either as an electric sensor or a magnetic loop. The diagram also shows the electric and magnetic preamplifiers, and the network used to bias the electric antenna. (The EP-5 package in OGO 4 and OGO 3 are similar but the earlier OGO's 1 and 2 did not have electric antenna nor bias network.)

The main body of OGO 3 (Figure 24) houses three narrowband sweeping receivers and two broadband receivers. Table 2 summarizes the main characteristics of the receivers on OGO 1 and OGO 3.

The sweeping receivers (bands 1, 2 and 3) measure the amplitudes of the detected signals, which are then digitized and telemetered by the wide band telemetry transmitter (WB TLM in the right margin of Figure 24). Band 1 covers the 3-octave range 0.2-1.6 kHz in 256 steps. At any step the frequencies of the band 1, band 2 and band 3 receivers are related as 1:8:64, so that together the three receivers cover the range 0.2-100 kHz. On command (mode 3, Table 3) the stepping receivers can be tuned

Table 2. Receiver characteristics of experiments A17 and B17

			Narrowbands			Broadbands	
			Band 1	Band 2	Band 3	VLF	ELF
Frequency range (kHz)		A17	0.2-1.6	1.6-12.5	12.5-100	0.3-12.5	*
		B17	"	"	"	"	0.015-0.300
Threshold sensitivity	magnetic field ($\mu\gamma$)	A17	240-30	24-3	1.6-0.2	30000-30	*
		B17	240-30	24-3	6-0.8	30000-30	10^6-10^4
	electric potential at input of preamplifier (μV)	A17	*	*	*	*	*
		B17	0.56	0.32	0.32	3.2	1.0
Dynamic range (db)		A17	90	90	80	80	*
		B17	90	90	80	80	90
Analog output (Volts)		A17	0-5	0-5	0-5		
		B17	0-5.12	0-5.12	0-5.12		
Local oscillator Freq. (kHz)			3.11-1.71	24.8-14.0	19.95-112		
IF Freq. (kHz)			3.31	26.5	212		
3-db Bandwidth (Hz)			40	160	600		
60-db Bandwidth (Hz)			450	1300	4500		
ΔF/step (Hz)			5.4	43	344		
Data rate (kbit/sec)			1,8,64	1,8,64	1,8,64		
Sweep rate (steps/sec)			1.68,13.9,111	1.68,13.9,111	1.68,13.9,111		
Sweep time (sec/sweep)			147,18.4,2.3	147,18.4,2.3	147,18.4,2.3		
Integration time constant(msec)			880,110,14	340,49,4.4	150,18,2		

*OGO 1 does not have electric antenna nor ELF receiver

Table 3. Modes of operation of experiments A 17 and B 17

MODE	Special Purpose Data (analog)					PCM data (digital)
	Channel 2			Channel 1		
	Local Oscillator of Band 2 (14-25 kHz)	Spectrum of broadband (0.3-12.5 kHz)	Band 3 phase (IF) (53 kHz)	VCO at 30 kHz ±7.5% contains:		Amplitudes in Bands 1, 2 and 3
				OGO 1 (A 17)	OGO 3 (B 17)	
1	always present at 1.25 V p-p	NO	NO	Amplitude of detected signals in VLF band (0.3-12.5 kHz)	Spectrum of ELF broadband (15-300 Hz)	sweeping
2		YES (3.75 V p-p)				
3		NO	YES (3.75 V p-p)	Amplitude of signal in Band 3		tuned at fixed frequency

to any fixed frequency within their range.

The broadband receivers yield the dynamic spectra of the log-compressed and clipped signals in the range 0.3-12.5 kHz (VLF receiver) and 20-300 Hz (ELF receiver, Figure 36). In mode 2 the VLF spectrum is transmitted in channel 2 of the special purpose (SP) telemetry (Table 3 and right margin of Figure 24). In modes 1 and 2 (OGO 3) the ELF spectrum frequency-modulates the voltage-controlled oscillator (VCO) at 30 kHz ±7.5%, which is transmitted in channel 1 of the SP telemetry (Table 3 and bottom right of Figure 24). (OGO 4 also had the ELF broadband receiver, although the earlier OGO's 1 and 2 did not.)

Calibration curves for OGO 1 and OGO 3 are shown in Figures 25-30 and 31-36 of Appendix B.

A detailed description of experiments A 17 and B 17 can be found in Rorden, et al [1966] and Ficklin, et al [1967b], respectively. The processing of the digital data from OGO 1 is described in Ficklin, et al [1967a].

III. EXPERIMENT PURPOSES

The proposed objectives of experiments A-17 and B-17, flown on OGO 1 and OGO 3 respectively, were to carry out in situ measurements that might lead to a better understanding of known VLF phenomena as well as to the discovery of new ones, and to make a comprehensive noise survey in the frequency range of 200 Hz to 100 kHz.

It was proposed that correlation between the satellite data and data received at a network of ground-based stations operated by Stanford University should prove useful. In particular, specific information was expected on:

1. The location of emission sources. This could be determined by studying the variation of emission characteristics with satellite location in the magnetosphere and also by comparing the satellite data with ground observations.

2. The relationship between ionospheric noise and magnetic storms.

3. The triggering of VLF emissions by whistlers and man-made signals.

4. The relationship of VLF phenomena to possible interactions, resonances and cutoffs in the plasma.

5. The validity of the magnetoionic duct theory of whistler-mode propagation and detailed characteristics of whistler-mode propagation.

6. Whistlers with anomalous spectra observed at Alouette but not on the ground.

7. The attenuation characteristics of whistler-mode paths, from measurements of the intensities of signals from VLF stations.

8. Variations of electron density with position, from observations of whistlers and man-made signals.

9. Electric field and ELF (30 Hz - 300 Hz) observations (OGO 3 only).

10. New VLF phenomena, in keeping with the exploratory nature of the experiments.

In the noise survey, it was proposed to include:

1. Terrestrial noises, such as those produced by lightning.

2. Noises generated within the ionosphere and magnetosphere, such as those produced by streaming particles, or triggered by whistler-mode waves.

The next section presents a concise account of the scientific achievements yielded to date by experiments A 17 and B 17, with specific references to the proposed research outlined above.

IV. RESULTS TO DATE

This section highlights the main scientific contributions of the research on the OGO-1 and OGO-3 data. The topics are organized in parallel with the experiment objectives outlined in the previous section. In general only a very brief description of results is made here, with a reference to the illustrated summaries in Appendix A. In a few cases, particularly with respect to current research not included in the Appendix, a more lengthy discussion is presented.

A. LOCATION OF EMISSION SOURCES

Four distinct types of noise were identified and studied in detail: banded chorus, whistler-mode emissions, high-pass noise and broadband noise.

Study of the variation with satellite position of the center frequency of the newly discovered banded chorus (Appendix A.7) indicated that these discrete emissions are generated inside the magnetosphere beyond the plasmapause and near the equatorial plane, at approximately half the local electron gyrofrequency. These conclusions support generation mechanisms involving doppler-shifted gyroresonance with energetic electrons. Banded chorus was also observed at ionospheric heights by OGO 2 in a frequency range that is consistent with the interpretation proposed here.

Both discrete and continuous whistler-mode emissions observed by OGO 1 were analyzed in detail (Appendix A.8). The experimental result that their upper cutoff is controlled by the equatorial gyrofrequency along the field line passing through the satellite is further evidence that these emissions originate near the magnetic equator. This study also reported the first intensity measurements of whistler mode emissions near the magnetic equator, which were found to be large enough to affect the electron fluxes

in the radiation belts. A strong space correlation found between high emission intensities and large electron fluxes is under further investigation with Vasyliunas of M.I.T.

Two new types of low frequency magnetic field noise were also discovered in the OGO-1 data: a broadband noise and a high-pass noise (Appendix A.9), both extending above the local gyrofrequency of electrons. These noises and the whistler-mode noise described above were found to be spatially anti-correlated.

Emissions in the magnetosheath were also observed by OGO 3, at frequencies between 1/4 and 5/8 the local electron gyrofrequency. The occurrence of these emissions is associated with fluctuations of the ambient magnetic field (Appendix A.10), particularly with its abrupt decrease. This phenomenon is still under investigation.

On 21 Jan 67 simultaneous observations of emissions were made at OGO 3 and at Byrd Station, Antarctica, near the southern foot of the field line passing through the satellite (see Appendix A.14 for the OGO 3 record). Further studies of this correlation are expected to yield more details of the generation process than heretofore possible.

B. RELATIONSHIP BETWEEN VLF PHENOMENA AND MAGNETIC DISTURBANCES

Several VLF phenomena were found to depend on magnetic activity. Among these, the banded chorus, described in Appendix A.7, occurs much more frequently when the value of K_p is above 2 than when it lies between 0 and 2.

Even more significantly, the onset of bursts of both highpass and broadband noises (Appendix A.9) observed in OGO 1 was found to coincide with the commencement of substorm activity as observed in the polar regions.

The time lapse between these onsets was less than 2 minutes, even when the satellite was beyond 18 earth radii.

A current study of MR (magnetospherically reflected) whistlers (see Appendices A.1, A.2 and A.5) shows that their occurrence is strongly dependent on the preceding magnetic activity. Thus, during several days after a large storm, when the plasmapause is gradually recovering from its low L value, it is observed that MR whistlers are barred from the recovery region between the innermost L-shell reached by the plasmapause and its "steady state" position, typically at $L = 4$ (Edgar, private communication).

Changes in whistler occurrence and noise characteristics across the plasmapause have been used to study that boundary in a correlative study (Appendix A.11) with Taylor's experiment on OGO 3.

C. TRIGGERING OF VLF EMISSIONS BY WHISTLERS AND MAN-MADE SIGNALS

At the OGO-1 and OGO-3 orbits the most common emissions excited by whistlers are those related to the highest frequencies in MR components (see for instance Figures 1 and 3 of Appendix A.1). These noises have been interpreted in terms of Landau growth due to a secondary peak in the electron energy spectrum (Appendix A.3). Due to the MR reflection near the lower hybrid resonance (LHR), emissions of this type are seldom observed at the polar OGO satellites, and were never received at ground stations.

Conversely, emissions of the type generally observed at the ground and triggered by whistlers or man-made signals are more commonly observed in the polar OGO's than at high altitudes. A discussion of these is given in the OGO-2 and OGO-4 report.

D. RELATIONSHIP OF VLF PHENOMENA TO INTERACTIONS, RESONANCES AND CUTOFFS IN THE PLASMA

The magnetospherically reflected (MR) whistlers provide evidence for

the reflection of VLF waves in the magnetosphere near the lower hybrid resonance (LHR) frequency (Appendices A.1, A.2 and A.5). The low frequency cutoffs of these whistlers were attributed to Landau damping due to a secondary peak in the electron energy spectrum (Appendix A.3).

An abrupt cutoff of signals from LF transmitters has been observed at OGO 1 near the local electron gyrofrequency (Appendix A.4). Current studies aim at ascertaining to what extent this phenomenon is due to absorption as opposed to defocusing near the resonance.

Several other resonance and cutoff phenomena have been discovered at low altitudes and are discussed in the OGO-2 and OGO-4 report.

E. VALIDITY OF THE MAGNETOIONIC DUCT THEORY; DUCT CHARACTERISTICS

A significant result from the OGO-1 and OGO-3 research was the confirmation of the existence of whistler ducts (Appendix A.1), determination of their physical characteristics, and verification of the predicted properties of whistler mode propagation along them (Appendix A.6). Among these, it is worthwhile to mention the interpretation of the upper cutoff of ground whistlers as untrapping rather than absorption, and the validity of both the strictly longitudinal approximation for ductec propagation and the hydrostatic model of the plasmasphere to calculate nose frequencies and travel times. Since most results based on ground whistler data rely on these assumption, this verification is of crucial importance.

F. WHISTLERS WITH ANOMALOUS SPECTRA

Study of OGO-1 data led to the discovery and interpretation of whistlers presenting "anomalous" dispersion, such as the MR and Nu whistlers (Appendices A.1, A.2 and A.5). Data from OGO 3 have also shown rising tones associated with ducted whistlers. Through ray tracings, these rising tones have been

interpreted as leakages from ducts that are beyond the satellite in L space (Appendix A.6).

Several other whistlers with anomalous spectra were observed at lower altitudes and are discussed in the OGO-2 and OGO-4 report.

G. ATTENUATION CHARACTERISTICS OF WHISTLER-MODE PATHS

Intensities of signals from VLF transmitters measured at the OGO 1 orbit were found in good agreement with theoretical predictions (Appendix A.13). A similar and more detailed study using OGO-4 VLF data is described in the OGO-2 and OGO-4 report.

H. VARIATION OF ELECTRON DENSITY WITH POSITION

Several characteristics of the VLF data have been used to detect variations of electron density with position. For instance, dispersion properties of Nu whistlers indicated that the electron density was a function of latitude at the time of the observations (Appendix A.5).

From in situ observations of whistler ducts several of their physical characteristics were determined for the first time. It was confirmed that they are enhancements of ionization, the relative enhancements ranging from 6% to 20% over the background. Their thicknesses in L space are of the order of 0.05 earth radii, and their widths in longitude 4 to 8 times as much at the equator (Appendix A.6).

Abrupt changes of whistler occurrence and noise characteristics were found across the plasmapause, as determined both by ion density measurements at the satellite and by whistler data from ground stations (Appendix A.11). This result not only evidences the changes in VLF activity across the plasmapause, but confirms the three dimensional nature of this boundary and establishes a new method for studying its characteristics. (A more complete study of this kind is described in the OGO-2 and OGO-4 report.)

A decrease in intensity of the high frequency inverter signals observed in inbound passes of OGO 1 coincides with the plasmapause crossing (Appendix A.12). This phenomenon is under study and may provide a very high resolution of the density profile across the plasmapause.

I. ELECTRIC FIELD AND ELF PHENOMENA (OGO-3 ONLY)

ELF (20 - 300 Hz) emissions were observed by OGO 3 in the magnetosheath. Their occurrence correlates with rapid variations of the local magnetic field, and their center frequency is near one quarter of the local electron gyrofrequency. These emissions were observed both by the electric and magnetic sensors of experiment B 17 (Appendix A.10). The interpretation of these observations is still under investigation.

J. NEW PHENOMENA

New VLF phenomena discovered in the OGO-1 and OGO-3 data and already discussed include:

- MR whistlers (Appendices A.1, A.2 and A.3).
- Nu whistlers (Appendices A.1 and A.5).
- leakages from ducts (Appendix A.6).
- banded chorus (Appendix A.7).
- highpass and broadband noise (Appendix A.9).
- ELF emissions in the magnetosheath (Appendix A.10).

Another new phenomenon, the super gyrofrequency (SG) whistler observed at OGO 3 outside the plasmapause (Appendix A.14), is still under investigation. The interpretation of this phenomenon relies on simultaneous ground data recorded near the foot of the field line passing through the satellite, at the Great Whale River Station in Canada and Byrd Station in Antarctica.

K. VLF NOISE SURVEY

A survey of the VLF noise observed by OGO 1 was carried out over

the first hundred orbits (Appendix A.8). The region surveyed includes all local times and the range of dipole latitudes from 0 to 50 degrees.

Figure 16 illustrates the maximum intensity of whistler mode noise (typically occurring below a few hundred Hertz) as function of local time and L-value. It shows two regions of high noise intensity in the dayside and a quiet region beginning at 00 LT and ending at 02 to 06 LT. (At low altitudes, OGO-4 data have also shown a marked decrease in ELF activity at these times (Crystal, private communication).) Outside the average position of the magnetopause, the intensity and occurrence of whistler-mode noise was observed to decrease. Noise up to several kHz has been observed at the shock boundary. Outside the shock little noise was observed, except for highpass noise as described below.

The survey also revealed two new kinds of noise, highpass and broadband noise, both extending above the local electron gyrofrequency. It was found that these noises and the whistler-mode noise are mutually exclusive (Appendix A.9).

A band of discrete emissions (banded chorus) was also observed outside the plasmapause, with a center frequency at 0.3 to 0.5 of the minimum gyrofrequency along the field line passing through the satellite (Appendix A.7).

V. APPENDIX A

Appendix A contains illustrated abstracts of research topics (both published and unpublished results).

A.1

MAGNETOSPHERIC PROPERTIES DEDUCED FROM OGO-1 OBSERVATIONS OF DUCTED AND NONDUCTED WHISTLERS (R. L. Smith and J. J. Angerami, J. Geophys. Res., 73, 1, 1968.)

The Stanford University/Stanford Research Institute VLF experiment on OGO 1 has revealed some basic features of both ducted and nonducted whistler-mode propagation in the magnetosphere. Two new types of whistler, the "magnetospherically reflected" and the "Nu" whistler were identified and qualitatively explained. Analysis of magnetospherically reflected and Nu whistlers provides support for the validity of Kimura's [1966] ray tracing results, and for the diffusive equilibrium model of the distribution of ionization along the geomagnetic field lines. In this study the first direct evidence of whistler "ducts" in the magnetosphere was obtained through analysis of the dispersion properties of a set of whistlers received on OGO 1.

Figure 1. OGO-1 frequency-time record of a "magnetospherically reflected whistler." The whistler results from dispersive propagation of lightning energy in the nonducted whistler mode in the magnetosphere. The separate traces result from successive reflections in the magnetosphere, as indicated roughly in Figure 2.

Figure 2. An example of one of many ray paths which produce the "magnetospherically reflected" whistler shown in Figure 1. The dispersion properties of the whistler result from propagation over a wide range of the magnetosphere and thus yield information on electron and ion densities over this range.

Figure 3. Complex forms of magnetospherically reflected whistlers and related phenomena. The whistlers shown here are obviously more complex than those shown in Figure 1. The complete explanation of these whistlers is yet to be found, but some preliminary results are discussed by Smith and Angerami [1968].

Reference

Kimura, I., Effects of ions on whistler-mode ray tracing, Radio Science, 1(new series), 269, 1966.

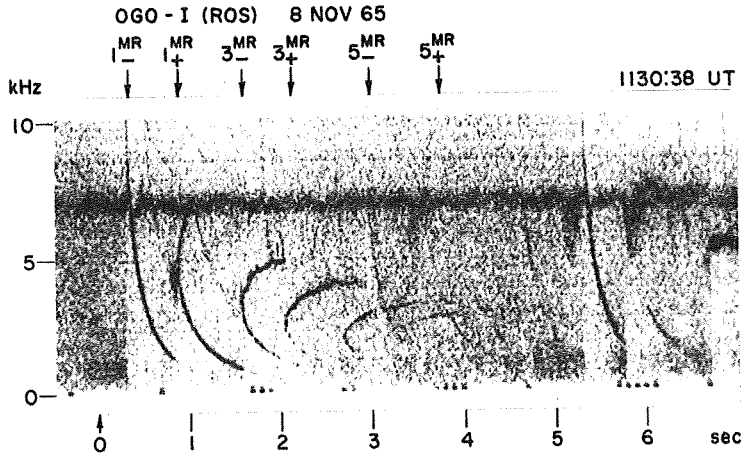

Figure 1

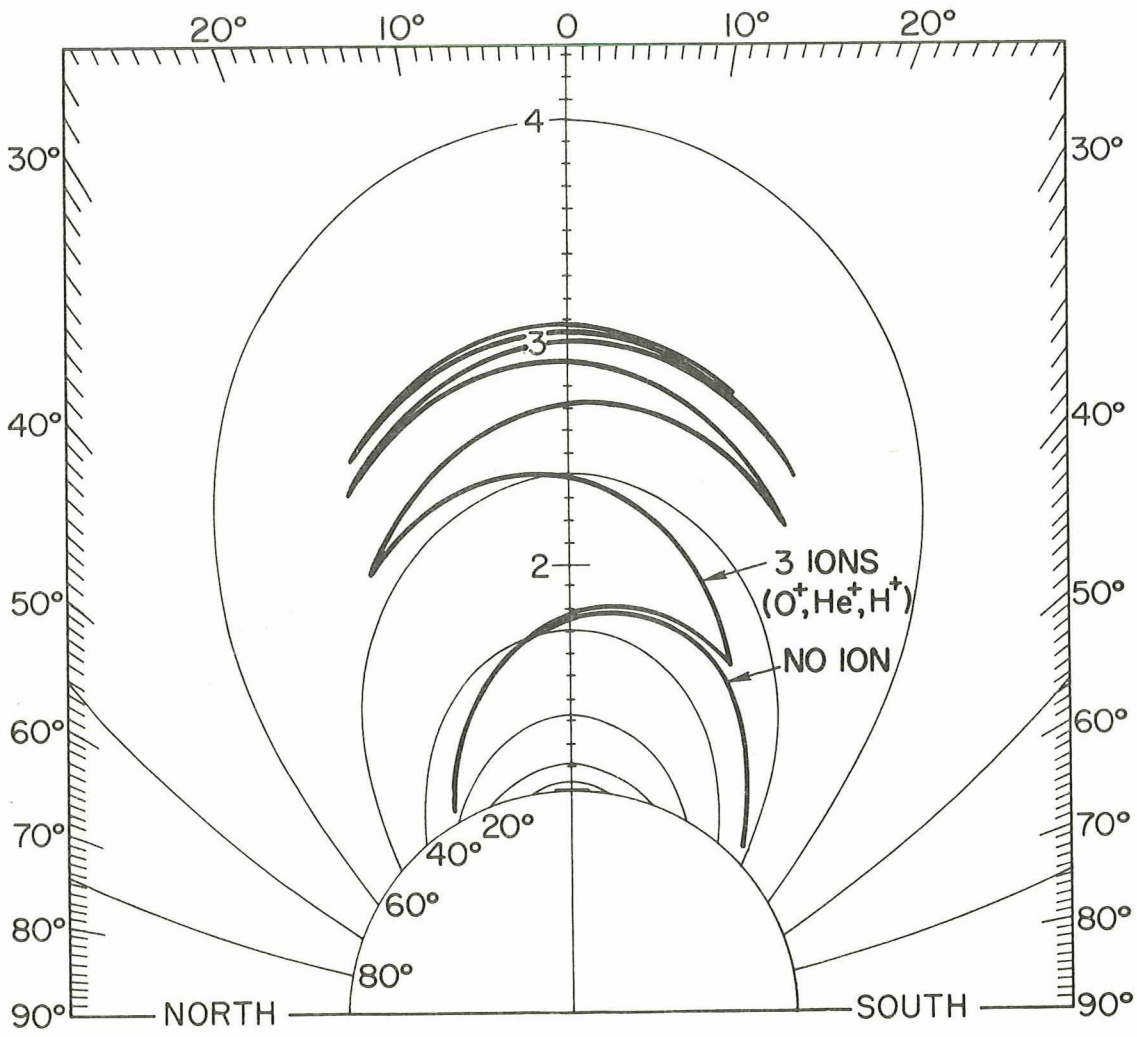

f = 1 kc/s
INITIAL WAVE NORMAL ANGLE = 0°
INITIAL LATITUDE = 30°N
D(I) MODEL

Figure 2

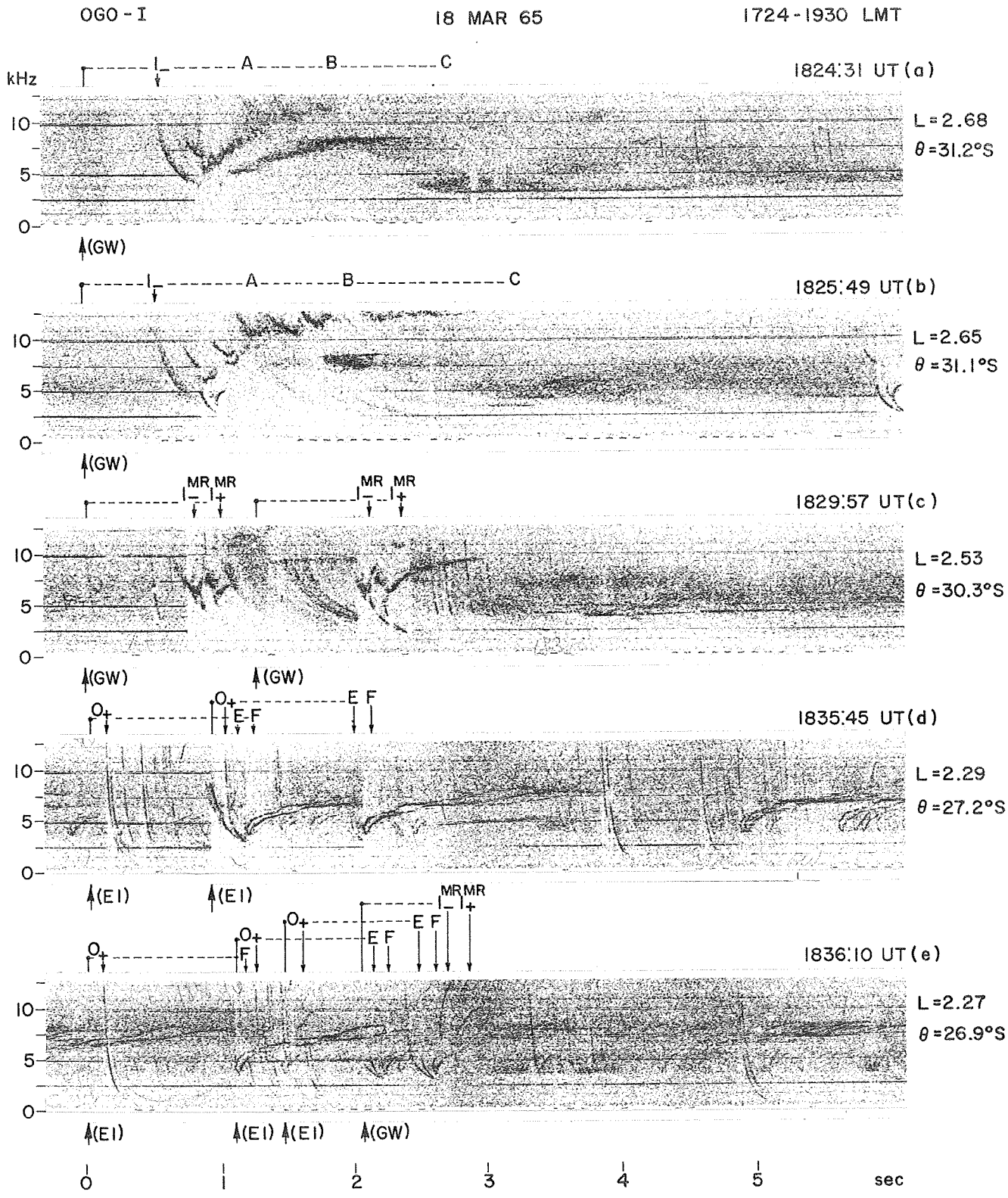
OGO - I
18 MAR 65
1724 - 1930 LMT
kHz
I
A
B
C
1824:31 UT (a)
L = 2.68
θ = 31.2°S
(GW)
1825:49 UT (b)
L = 2.65
θ = 31.1°S
MR MR
MR MR
1829:57 UT (c)
L = 2.53
θ = 30.3°S
O+
E-F
E F
1835:45 UT (d)
L = 2.29
θ = 27.2°S
(EI)
F
1836:10 UT (e)
L = 2.27
θ = 26.9°S
10
5
0
0
1
2
3
4
5
sec

Figure 3

A.2

THE MAGNETOSPHERICALLY REFLECTED WHISTLER (B. Edgar, research in progress.)

A common form of nonducted whistler observed by OGO's 1 and 3 inside the plasmasphere is the magnetospherically reflected (MR) whistler. The frequency-time spectrograms of a succession of four MR whistlers are shown in Figure 4 (see also Figure 1). Each MR whistler consists of many components characterized by low (2-4 kHz) "nose" frequencies. The first component has an Eckersley's law dispersion and is a nonducted fractional-hop whistler which entered the base of the ionosphere at $\sim 30^{o}$N. The second component is formed by a nonducted whistler which starts at $\sim 25^{o}$N and propagates roughly along the magnetic field line. The wave normal of this whistler tends to lag behind the earth's magnetic field and approaches 90^{o}. As long as the frequency of the signal is greater than the local lower hybrid frequency (LHR), the whistler ray path closely follows a magnetic field line across the magnetic equator at $L \sim 2$ and into the southern hemisphere. As soon as the LHR becomes higherthan the frequency of the whistler, the refractive index surface closes at 90^{o} and allows the whistler ray to be refracted and its direction to be reversed. Since the refraction process occurs in a small region, it is called a "reflection"; thus the origin of the term "magnetospherically reflected whistler." After being reflected, the whistler propagates towards the magnetic equator, where it is eventually observed by the satellite at $L \sim 2.5$. The third component is formed by a whistler which undergoes a reflection in the southern hemisphere, propagates into the northern hemisphere, and undergoes a reflection there. After the second reflection the whistler is observed in the equatorial

region by the satellite. Accordingly, the higher order components undergo many reflections before being observed by the satellite. The changes in the spacing pattern between individual components are caused by the relative shortening and lengthening of ray paths as the satellite changes latitude.

Raytracings were successfully used in the interpretation of MR whistlers. Figure 4 shows the good agreement achieved between the travel times observed and calculated by tracing rays in a model magnetosphere. Ray tracing studies of MR whistlers have also shown that their spectra embody information about the structure of the inner magnetosphere. Thus, they are very valuable in evaluating changes in the magnetosphere such as due to magnetic storms.

Figure 4. Frequency-time spectra of a sequence of MR whistlers illustrating the change in spacing between components as the satellite moves from the southern to the northern hemisphere. The causative lightning sources were located in the northern hemisphere. The solid lines represent the actual MR whistlers observed, and the dotted lines and circles represent the calculated time delays computed by ray tracing. The density model used was a simple diffusive equilibrium with 50% H^+ and 50% O^+ at a 1000 km altitude. The small time delay discrepancies above the nose frequencies are due to the fact that the model does not include all of the vertical and horizontal gradients present along the whistler ray paths.

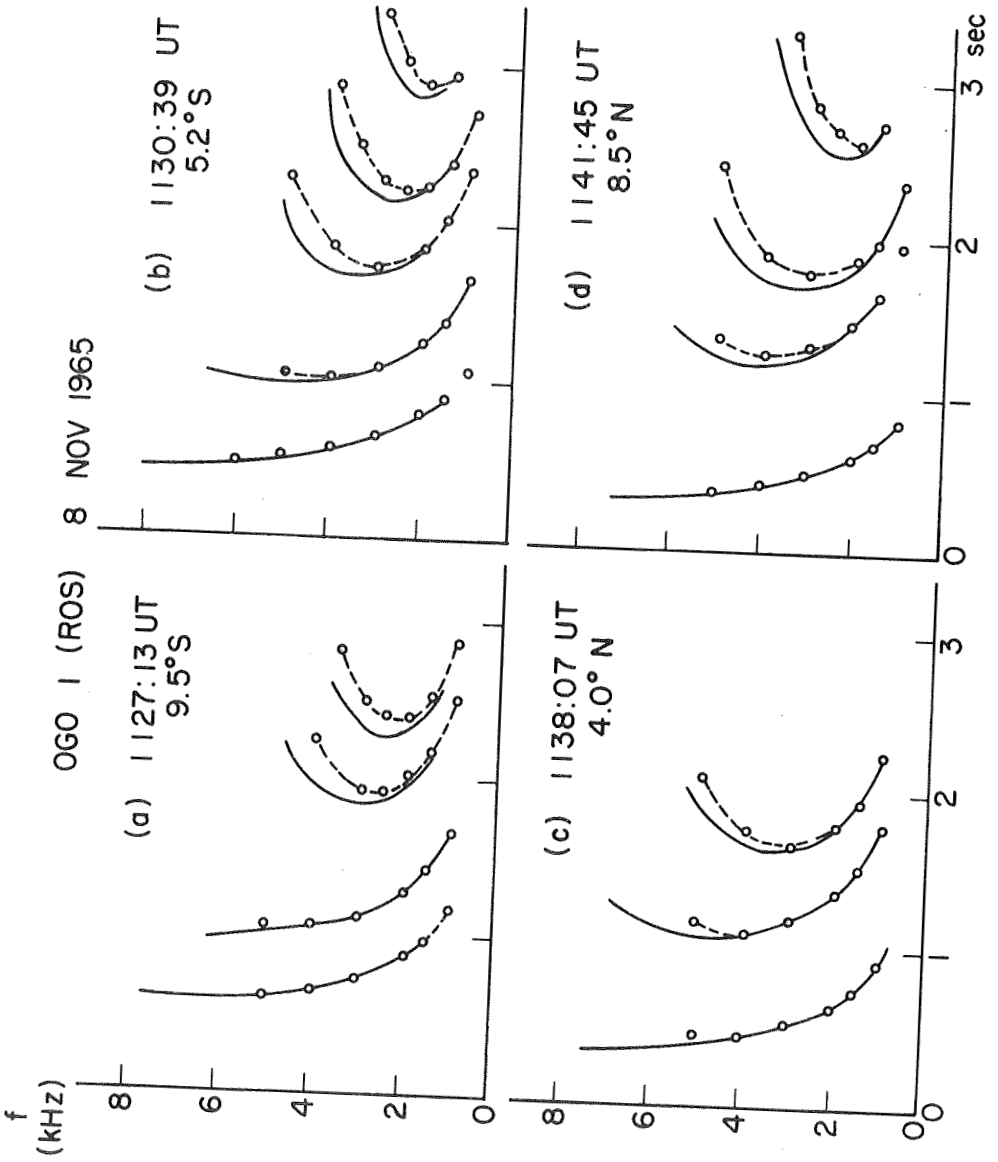
OGO I (ROS) 8 NOV 1965
(a) 1127:13 UT
9.5°S
(b) 1130:39 UT
5.2°S
(c) 1138:07 UT
4.0° N
(d) 1141:45 UT
8.5°N
f
(kHz)
8
6
4
2
0
1
2
3
sec

Figure 4

A.3

UNDUCTED WHISTLER EVIDENCE FOR A SECONDARY PEAK IN THE ELECTRON ENERGY SPECTRUM NEAR 10 KEV (R. M. Thorne, J. Geophys. Res., 73, 4895, 1968.)

The upper and lower frequency cutoffs as well as certain growth features of magnetospherically-reflected whistlers are explained in terms of Landau damping by an ambient electron distribution that has a secondary peak in the vicinity of 10 kev.

A.4

ABRUPT CUTOFF OF WHISTLER-MODE SIGNALS NEAR THE LOCAL ELECTRON GYROFREQUENCY (N. Dunckel and R. A. Helliwell, research in progress.)

Signals from low-frequency ground-based transmitters are commonly observed in the output of the band 3 sweeping receiver on OGO 1. On outbound passes, transmissions in the range 70-100 kHz are often observed to drop sharply in intensity when f/f_H, the ratio of signal frequency to local electron gyrofrequency, rises to ~ 0.9. Figure 5 shows the intensity of signals from a transmitter at 82 kHz together with f_H versus time. Near 1042 UT the observed signals drop 20 db, reaching the threshold level. At this time $f/f_H = 82.0/87.5 = 0.94$. Fluctuations prior to this decrease may be due to multi-path fading. Studies are presently underway to ascertain if the sharp decrease may be caused by the increasing divergence of rays as f_H approaches the signal frequency or if it may be caused by Landau damping.

Figure 5. Abrupt decrease of signal intensity from ground-based transmitter as f_H, the local electron gyrofrequency, near signal frequency. Plot shows intensity of signal in db above 1 gamma rms at 82 kHz recorded on an outbound pass versus universal time. Variation of f_H at the satellite is also plotted from ephemeris. Signal intensity drops about 20 db at 1041:51, when $f_H = 87.5$ kHz. Thereafter signal lies below threshold of receiver. Data were recorded December 23, 1964. At 1041 UT the satellite was at $L = 3.8$ and at a magnetic latitude of 38^o.

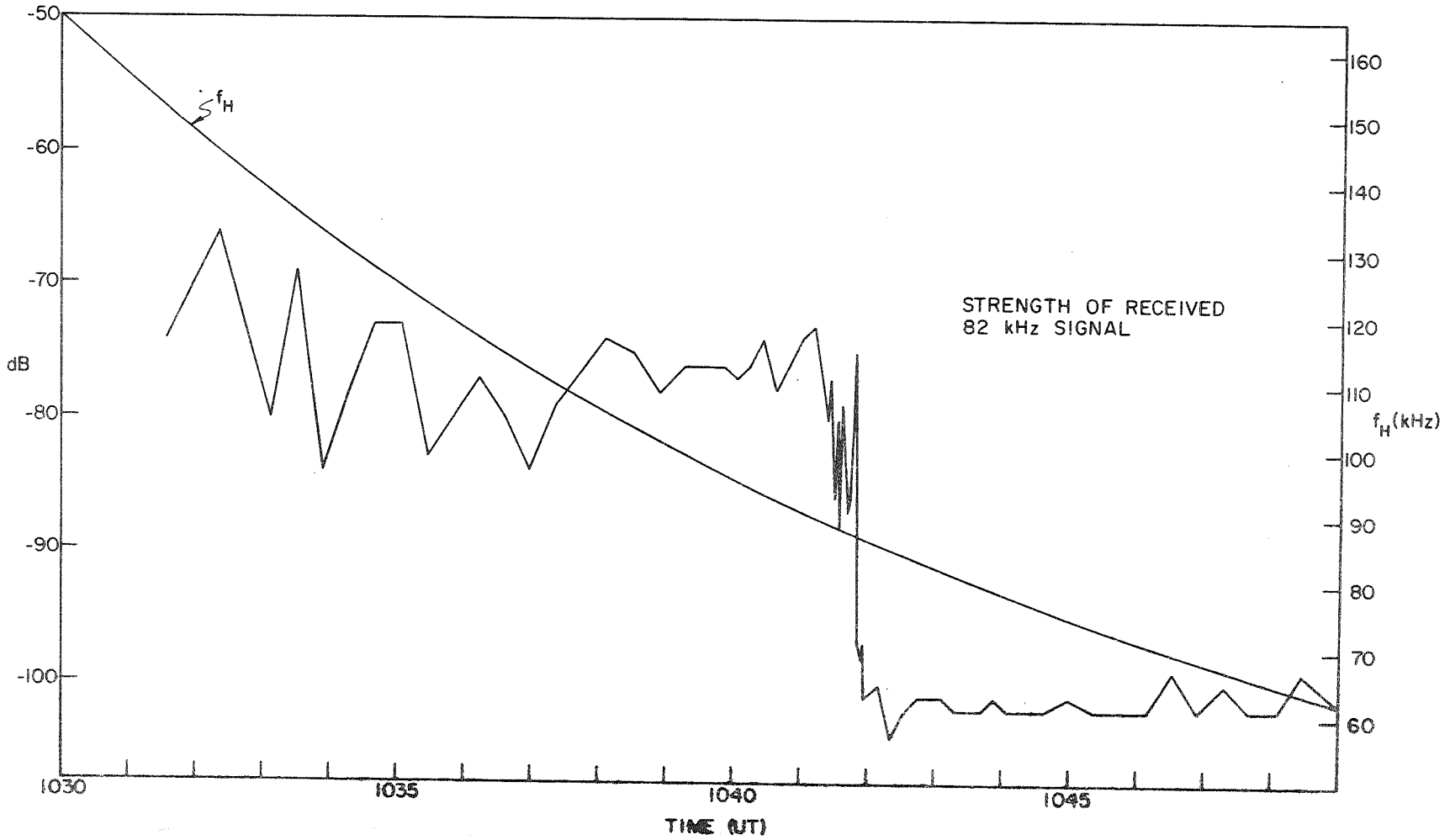
-50
-60
-70
-80
-90
-100
dB
160
150
140
130
120
110
100
90
80
70
60
f_H(kHz)
f_H
STRENGTH OF RECEIVED
82 kHz SIGNAL
1030
1035
1040
1045
TIME (UT)

Figure 5

A.5

APPLICATION OF THE NU WHISTLER TO MAGNETOSPHERIC DENSITY PROFILES
(B. Edgar, research in progress)

At latitudes of 25 to 30° the separate traces of the magnetospherically-reflected whistler (see items A.1 and A.2) are frequently joined at a minimum frequency, resulting in the "Nu" whistler. An example of the Nu whistler is shown in Figure 6. The position of the reflection of the lowest Nu-whistler frequency is known to be near the satellite, and from this added information we have shown that at the time these data were recorded the model of ionization density in the magnetosphere included a dependence on latitude (see Figure 7). By applying more sophisticated models, including a latitudinal dependence, additional detail on the plasma density distribution is being obtained.

Figure 6. Frequency-time record of a "Nu" whistler received on OGO 1. The whistler trace between 1 and 2 sec has the appearance of the reverse of the Greek letter ν and is termed a "Nu" whistler. The joining or minimum frequency of the Nu whistler is approximately 1.7 kHz.

Figure 7. Result of ray tracing in the magnetosphere for waves at 1.7 kHz. The dashed curves show the ray path and the locus of possible reflection points for the joining frequency of a Nu whistler based on a plasma density model having no variation with latitude. The solid curves show a ray path and locus of possible reflections for a field-aligned model having a base level variation of density as shown in the lower part of the figure.

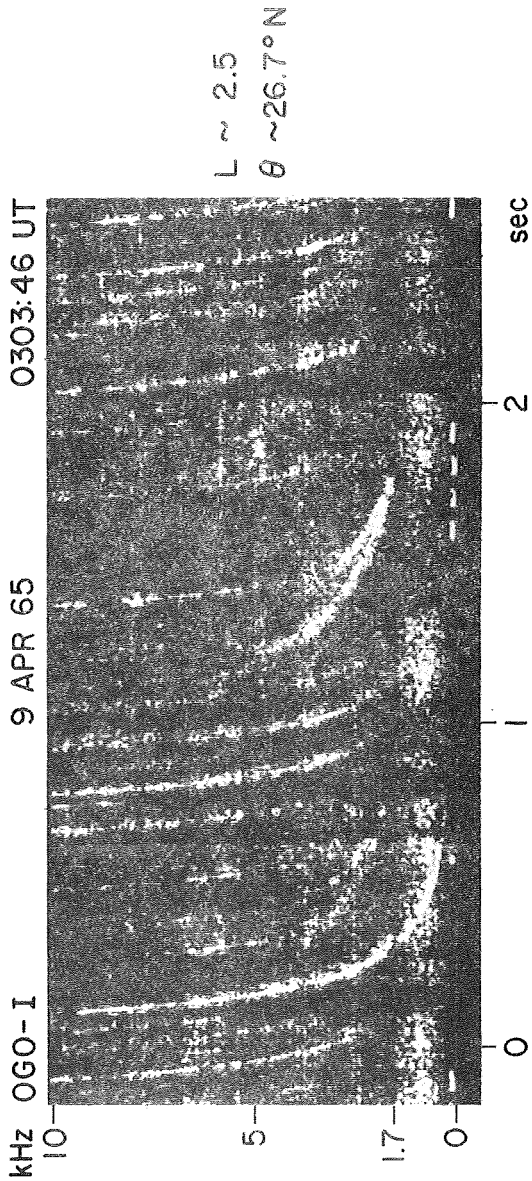

Figure 6

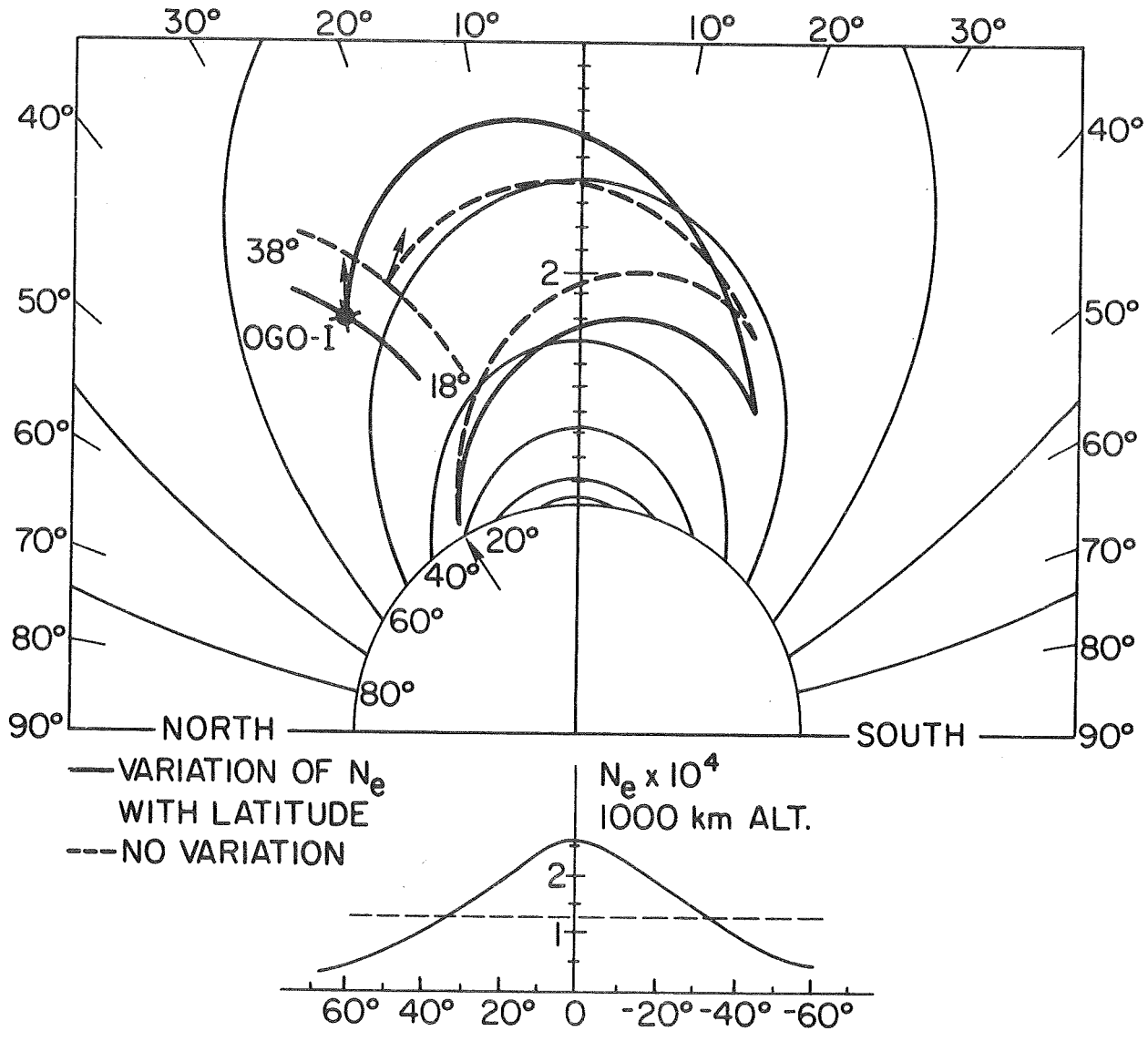
30°
20°
10°
10°
20°
30°
40°
50°
60°
70°
80°
90°
38°
OGO-I
18°
2
20°
40°
60°
80°
NORTH
SOUTH
—VARIATION OF N_e
WITH LATITUDE
---NO VARIATION
$N_e \times 10^4$
1000 km ALT.
2
1
60° 40° 20° 0 -20° -40° -60°

Figure 7

A.6

WHISTLER DUCT PROPERTIES DEDUCED FROM VLF OBSERVATIONS MADE WITH THE OGO-3 SATELLITE NEAR THE MAGNETIC EQUATOR (J. J. Angerami, submitted to J. Geophys. Res., 1970)

While the great majority of ground whistlers are interpreted as indirect evidence of magnetospheric ducts, the first direct evidence of ducts was obtained from the Stanford broadband VLF experiments on OGO 1 [Smith and Angerami, 1968] and OGO 3. The present paper is a case study of OGO-3 duct observations made during the inbound pass of 15 June 1966. On this pass five discrete whistler ducts were encountered by OGO 3 between $L = 4.7$ and 4.1. Each duct was characterized by reception at the satellite of ducted whistlers with a distinct spectral shape, along with the high-frequency portions of whistlers (leakages) that propagated inward from outer ducts. Figure 8 shows a model of the propagation paths and corresponding spectra. Figure 9 illustrates actual data received in the fifth duct traversed.

The data were interpreted in detail by ray tracing in a model magnetosphere that includes ducts of enhanced ionization. As an illustration, Figure 10 shows the calculated ray trajectory of a leakage from the second to the fifth duct. The frequency is 8.7 kHz, corresponding to the highest frequency of L_2 in Figure 9. The calculated and observed travel times agree within five percent.

Analysis of the data yielded the following conclusions:

1. The L-shell thicknesses of the observed ducts ranged between 0.035 and 0.070 earth radii, and the interduct separations ranged between 0.017 and 0.18 earth radii.
2. The dimension of the ducts in longitude was estimated to be on the order of 4^{o}, or 0.3 earth radii at the equator, a factor of $\sim$ 4-8 greater than the L-shell dimensions. Figure 11 shows a cross section model of the duct distribution which is consistent with the present observations and with ground occurrence of whistlers.

3. The whistler ducts are much more likely to be enhancements than troughs.

4. The minimum enhancement factors needed to trap frequencies up to half the electron gyrofrequency are on the order of 6%, smaller values producing upper cutoffs at frequencies below half the gyrofrequency. Analysis of electron density equatorial profiles determined by ground whistlers indicates that the enhancement in ducts is generally less than 22%. The radial variation of electron density used in the calculations is shown in Figure 12, where enhancements of 10% were initially assumed and then readjusted (ducts no. 2 and 3) to fit all observed travel times.

5. The upper cutoff of ground whistlers is a trapping (rather than absorption) effect.

6. The hydrostatic type of distribution of ionization along the field lines is applicable in the plasmasphere.

7. The travel times (and frequency of minimum delay) of ducted whistlers can be calculated with good accuracy by assuming purely longitudinal propagation.

The data also show that the leaked signals are confined in space; the cross section of a tube of rays spreads by only a factor of 3 after leaking from the duct. This explains the high intensity of the leakages. The limited spreading has been confirmed by ray tracing, and is due to the electromagnetic guiding produced by the anisotropy, especially as the wave frequency approaches the gyrofrequency.

Figure 8. To illustrate ray trajectories of ducted whistlers and inward leakages from outer ducts. Sketch (a) shows the snake-like ray trajectories typical of ducted propagation at frequency f below half the gyrofrequency. The satellite at S_o in the outer duct receives a whistler whose time-frequency spectrum is shown in (b). Sketch (c) shows a ray trajectory in the outer duct at a frequency f' equal to half the gyrofrequency at point A. Beyond A there is no trapping and the ray bends inward, producing a leakage L_o observed by the satellite at S_i. The corresponding time-frequency spectrum is shown by L_o in (d) together with the whistler D_i, which is ducted along the inner duct.

Figure 9. Example of time-frequency spectrum of whistler signals received by OGO-3 while crossing the fifth (innermost) duct. D_5 is the whistler ducted along the fifth duct. L_4, L_3 and L_2 are the high frequency leakages from the next three outer ducts (cf. Figure 8c,d). The horizontal lines are interference from the rubidium vapor magnetometer aboard OGO 3 and represent

one quarter of the local electron gyrofrequency and its harmonics.

Figure 10. Ray trajectory calculated to explain the highest frequency of the leakage from the second duct observed by OGO 3 in the fifth duct traversed (L_2 in Figure 9). Beyond point A, where the wave frequency equals half the local gyrofrequency ($\lambda = 0.5$), the wave normals (arrows) tend to turn outward with respect to the geomagnetic field and the ray turns inward. These effects are most pronounced beyond point B.

Figure 11. A model of equatorial cross section of whistler ducts. The heavy-shaded ducts were actually observed by OGO 3, whose orbit is shown by the dashed line. The dashed contours represent ducts inferred to exist assuming that the ducts encountered one part of a random distribution in space. The longitude width of the ducts is probably accurate within a factor of 2; it was inferred by setting a lower limit based on the absence of leakages from neighboring ducts, such as A and B, and an upper limit based on a comparison between whistler occurrences in satellite and ground data.

Figure 12. Equatorial profile of electron density. The continuous line represents the model used in the calculations. Different enhancements in the second and third ducts were used to fit the observed travel times. The open circles represent values of density calculated from whistlers received at Byrd Station, Antarctica, 73° west of the OGO-3 meridian.

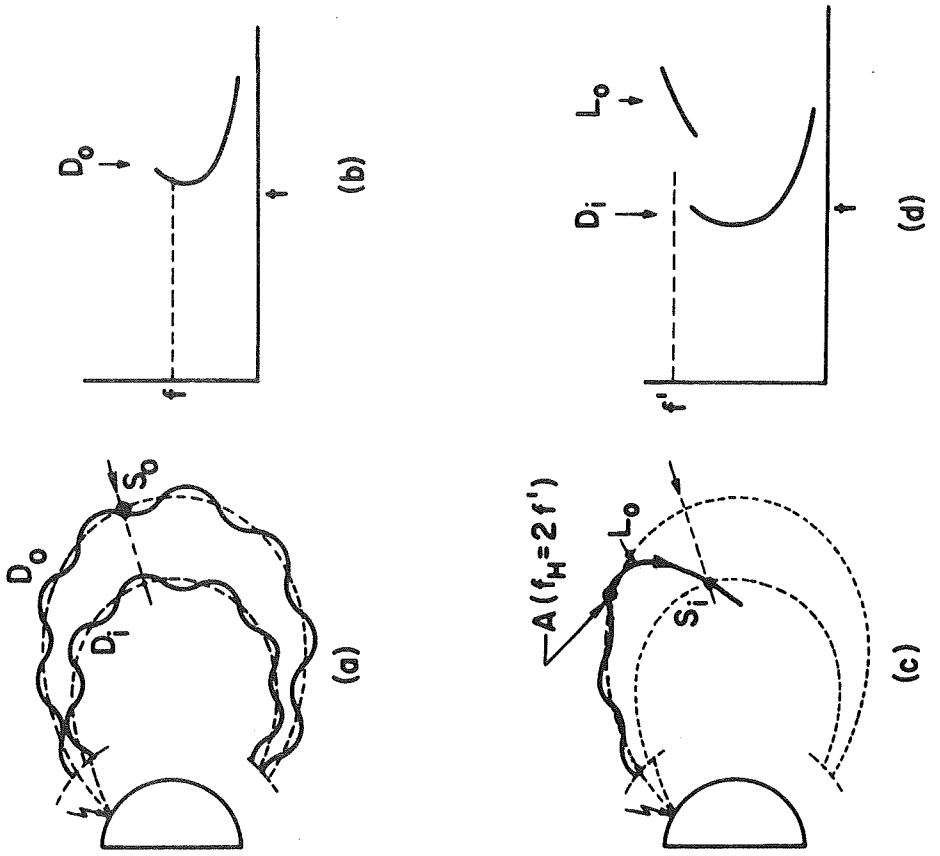

Figure 8

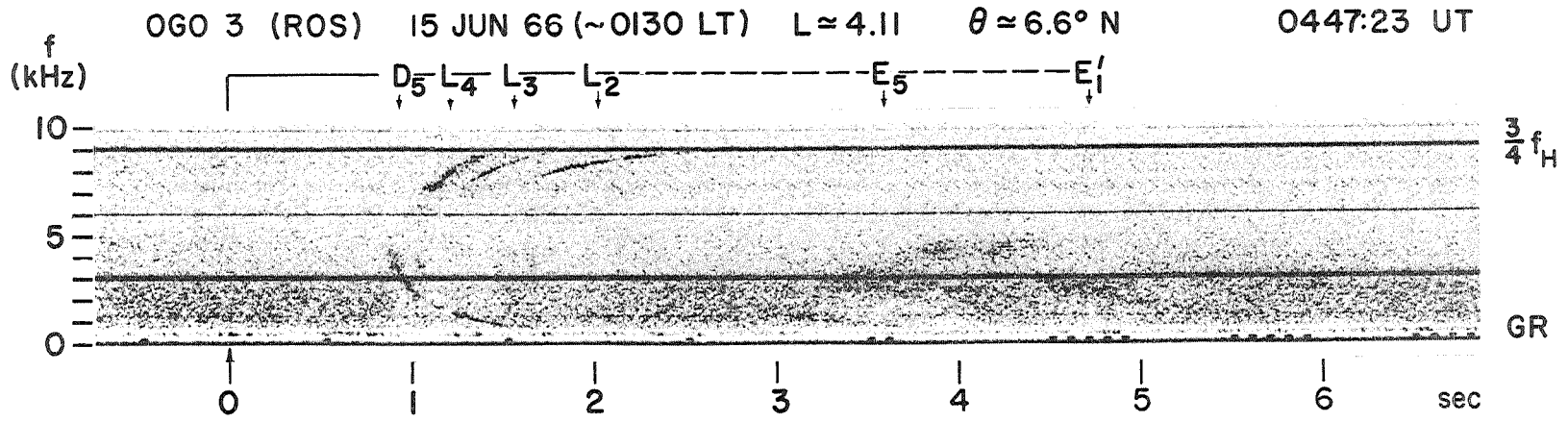
OGO 3 (ROS) 15 JUN 66 (~0130 LT) L≃4.11 θ≃6.6° N 0447:23 UT
f (kHz)
D5 L4 L3 L2 E5 E'1
10
5
0
3/4 fH
GR
0 1 2 3 4 5 6 sec

Figure 9

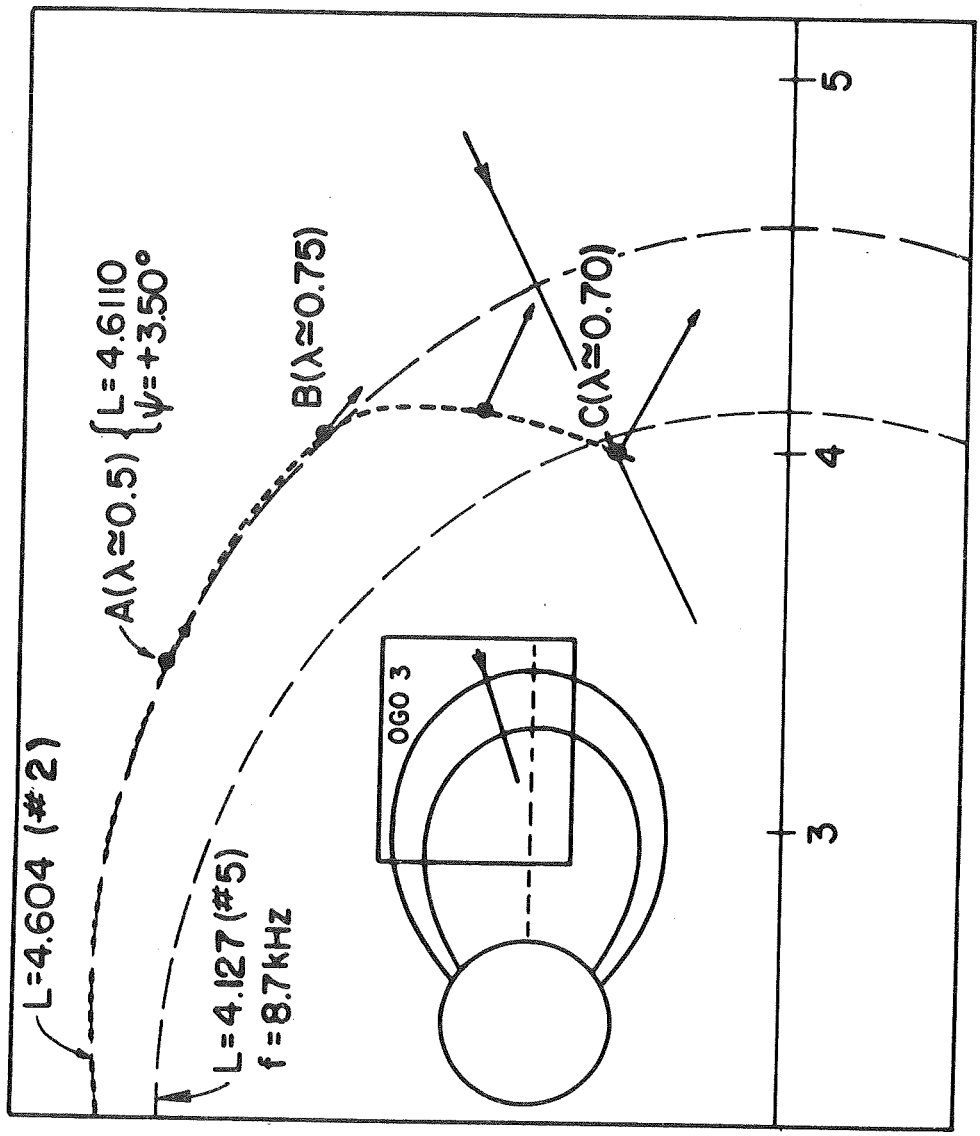

Figure 10

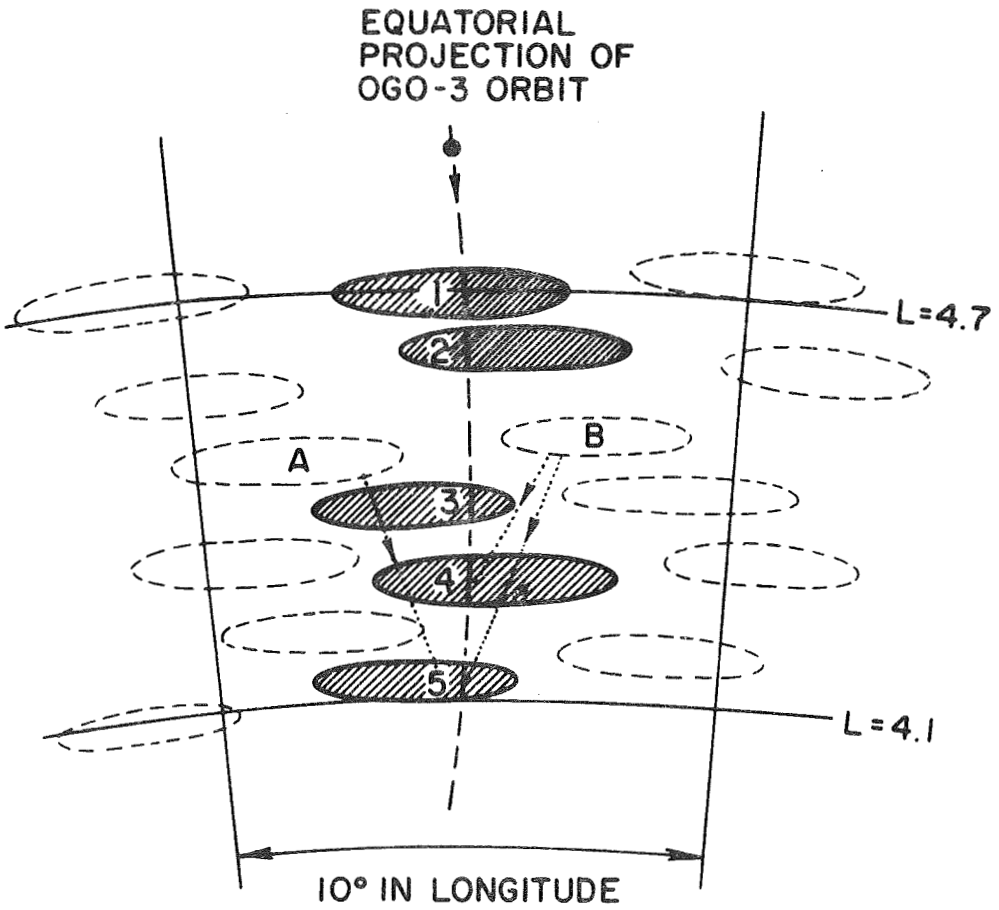
EQUATORIAL
PROJECTION OF
OGO-3 ORBIT
L=4.7
L=4.1
A
B
1
2
3
4
5
10° IN LONGITUDE

Figure 11

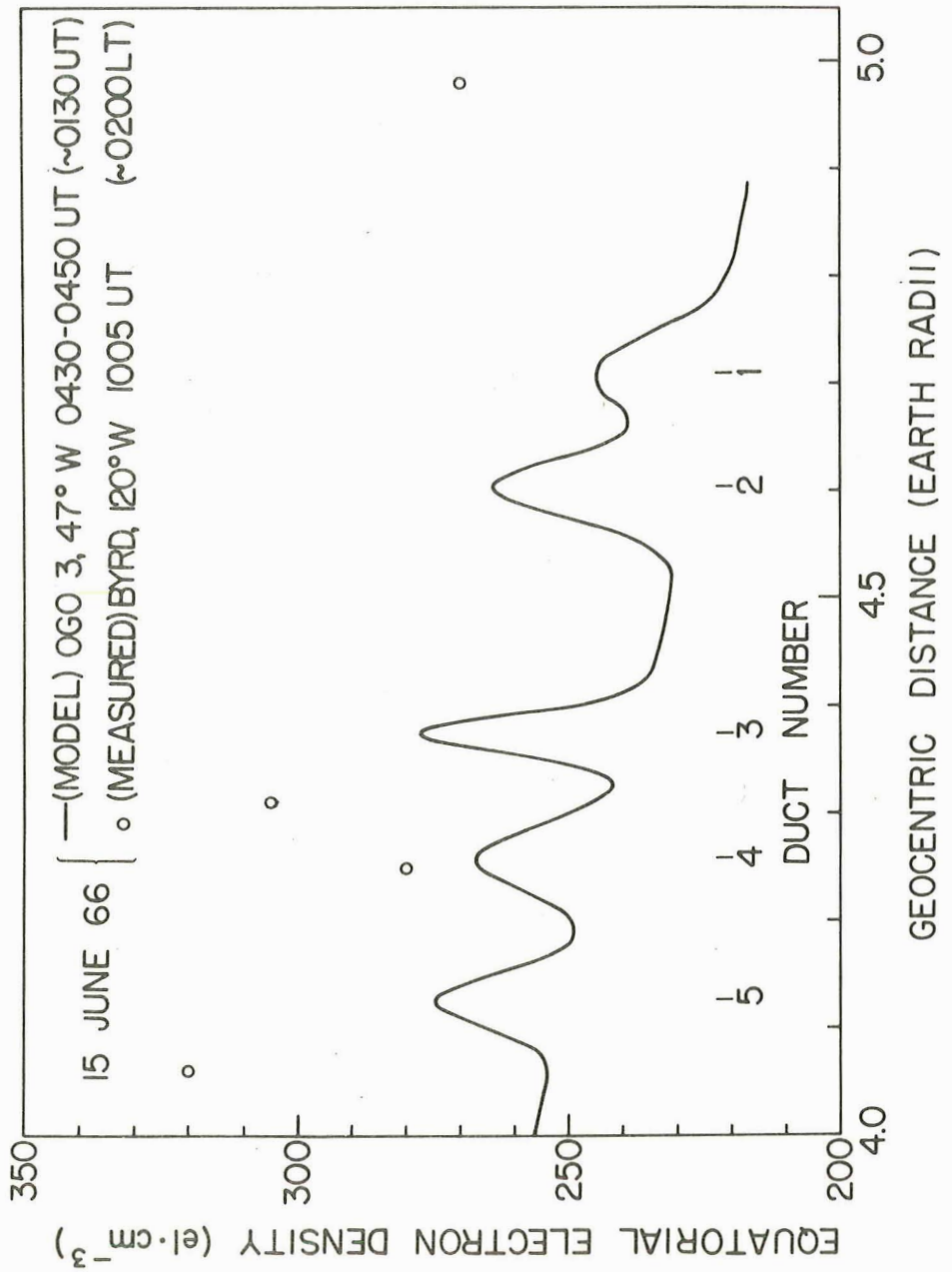
15 JUNE 66
—(MODEL) OGO 3, 47° W 0430-0450 UT (~0130 UT)
o (MEASURED) BYRD, 120° W 1005 UT (~0200 LT)
EQUATORIAL ELECTRON DENSITY (el·cm⁻³)
350
300
250
200
4.0
4.5
5.0
GEOCENTRIC DISTANCE (EARTH RADII)
DUCT NUMBER
1/5
1/4
1/3
1/2
1/1

Figure 12

A.7

BANDED CHORUS--A NEW TYPE OF VLF RADIATION OBSERVED IN THE MAGNETOSPHERE BY OGO 1 AND OGO 3 (W. Burtis and R. A. Helliwell, J. Geophys. Res., 74, 3002, 1969; W. Burtis, Engineering Thesis.)

The Stanford University/Stanford Research Institute VLF experiments on OGO 1 and OGO 3 have provided important new information on the nature of the 'chorus' type of discrete VLF emission. Naturally occurring chorus emissions have for some years been observed at ground stations, and a number of theories have been advanced to explain their origin. Because of propagation factors there are significant differences between the emissions observed on the ground and those observed in the magnetosphere. In the present study the latter are found to occur primarily in a single, spatially varying frequency band and are termed "banded chorus". From analysis of banded chorus, it is concluded that the emissions are generated in the equatorial plane of the earth at distances from 3 to 10 earth radii, and that the generation occurs at approximately half the electron gyrofrequency. The latter conclusion supports those generation theories involving doppler-shifted gyroresonance with trapped electrons.

The OGO-1 and OGO-3 observations also show that banded chorus emissions do not propagate exactly along magnetic field lines. The actual raypath has been explained in terms of nonducted propagation in a model magnetosphere. Depending on the ambient properties of the magnetosphere and topside ionosphere, banded chorus may or may not be observable at the lower altitudes of OGO 2 and OGO 4. These satellites provide an important link between the observations of discrete VLF emissions in the magnetosphere and on the ground. As the understanding of VLF emissions becomes more complete, their analysis leads to new information regarding

both energetic and ambient thermal particle distributions in the plasma trough.

Figure 13. OGO-1 frequency-time record showing that the frequency of a band of VLF emissions (banded chorus) is strongly related to f_{Ho}, the equatorial electron gyrofrequency on the field line passing through the satellite. The banded chorus frequency is evidently <u>not</u> related to the local electron gyrofrequency f_H.

Figure 14. A computed raypath based on nonducted propagation in model magnetosphere. The inward deviation of the raypath from the magnetic lines is in general agreement with the OGO-1 and OGO-3 observations of banded chorus.

Figure 15. A noise band closely resembling the banded chorus seen by OGO 1 is observed in the topside ionosphere by OGO 2. Such observations are relatively rare and occur only during magnetically disturbed periods.

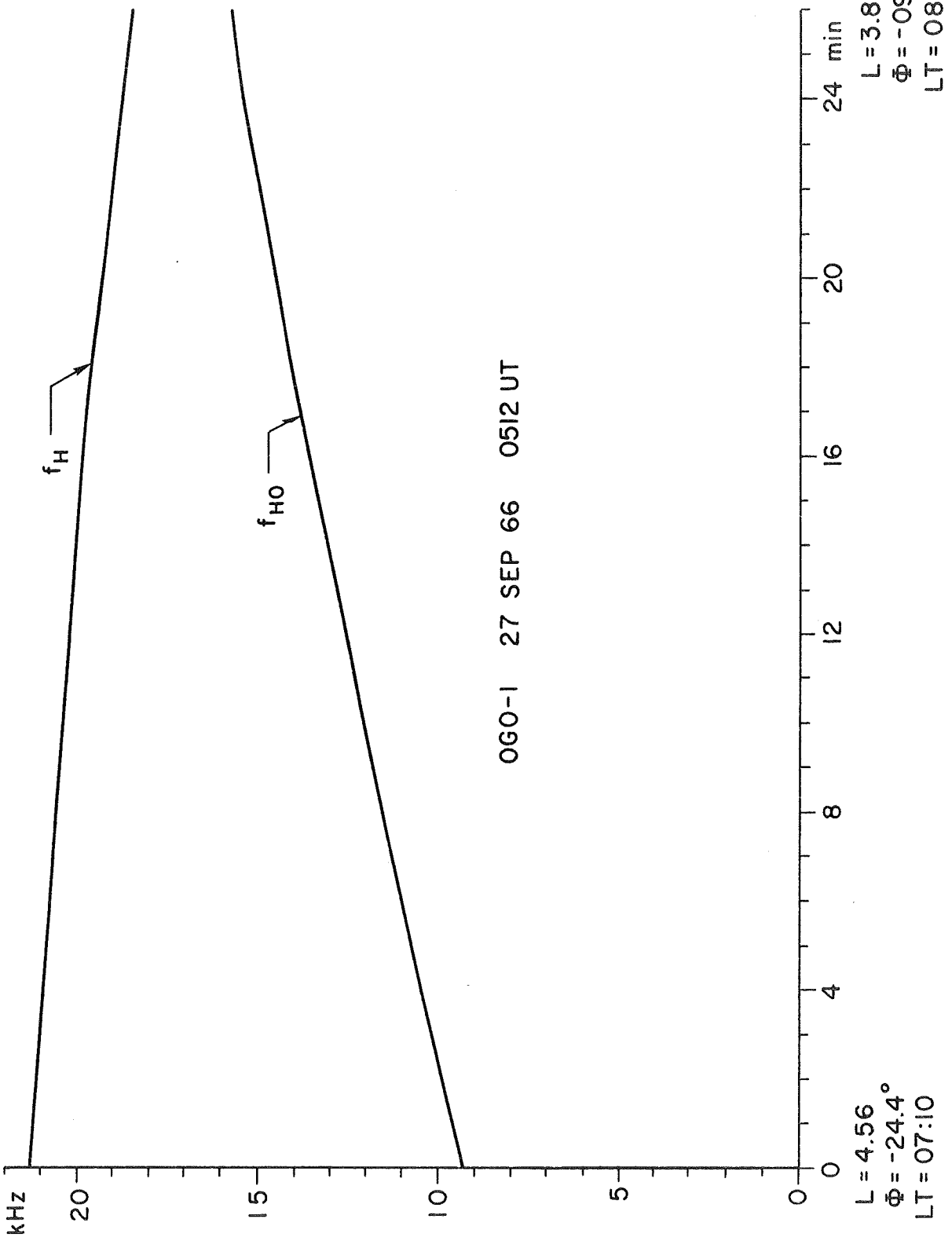
kHz
20
15
10
5
0
f_H
f_{HO}
OGO-I 27 SEP 66 0512 UT
0
4
8
12
16
20
24 min
L = 4.56
Φ = -24.4°
LT = 07:10
L = 3.83
Φ = -09.9°
LT = 08:10

Figure 13

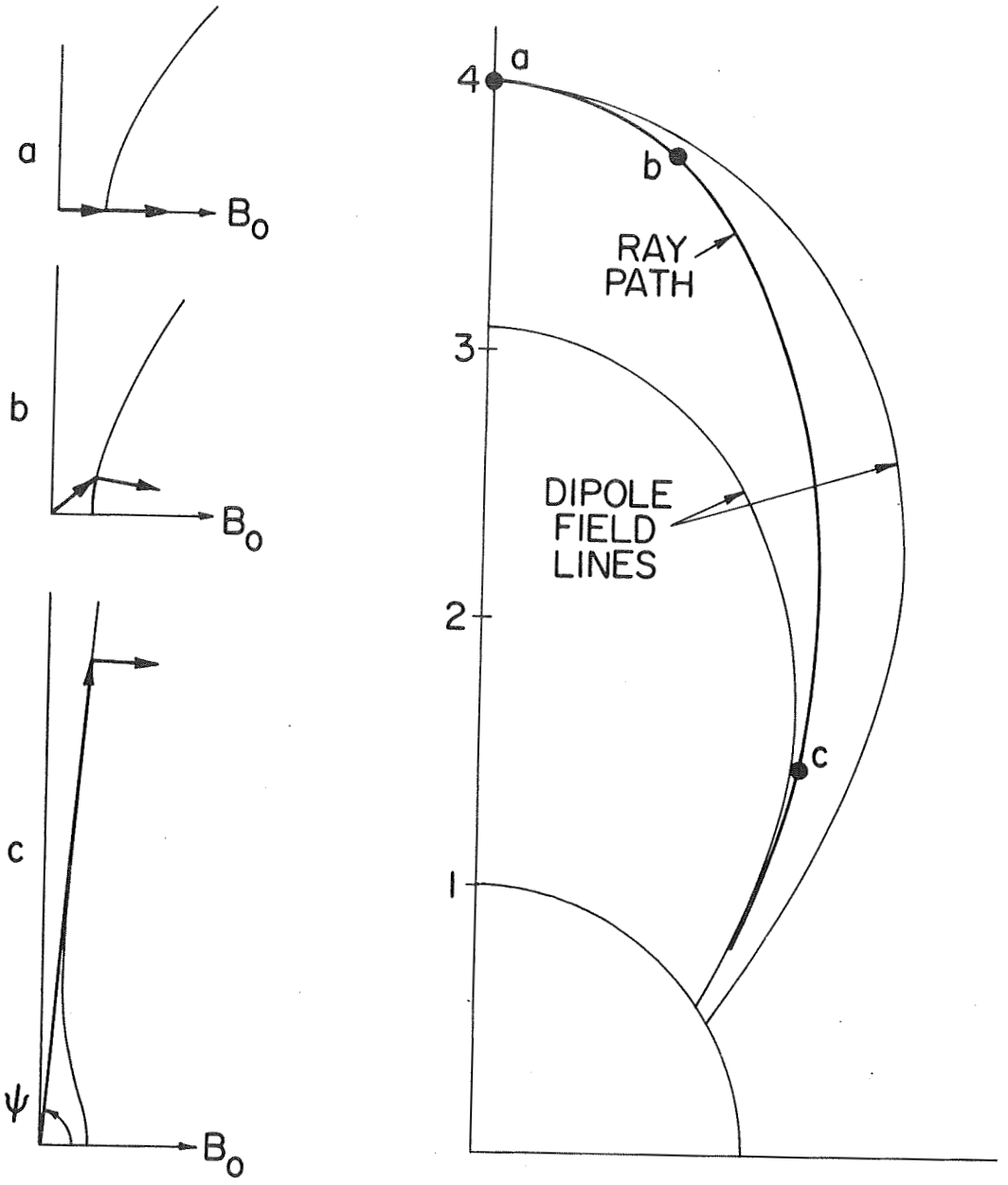

Figure 14

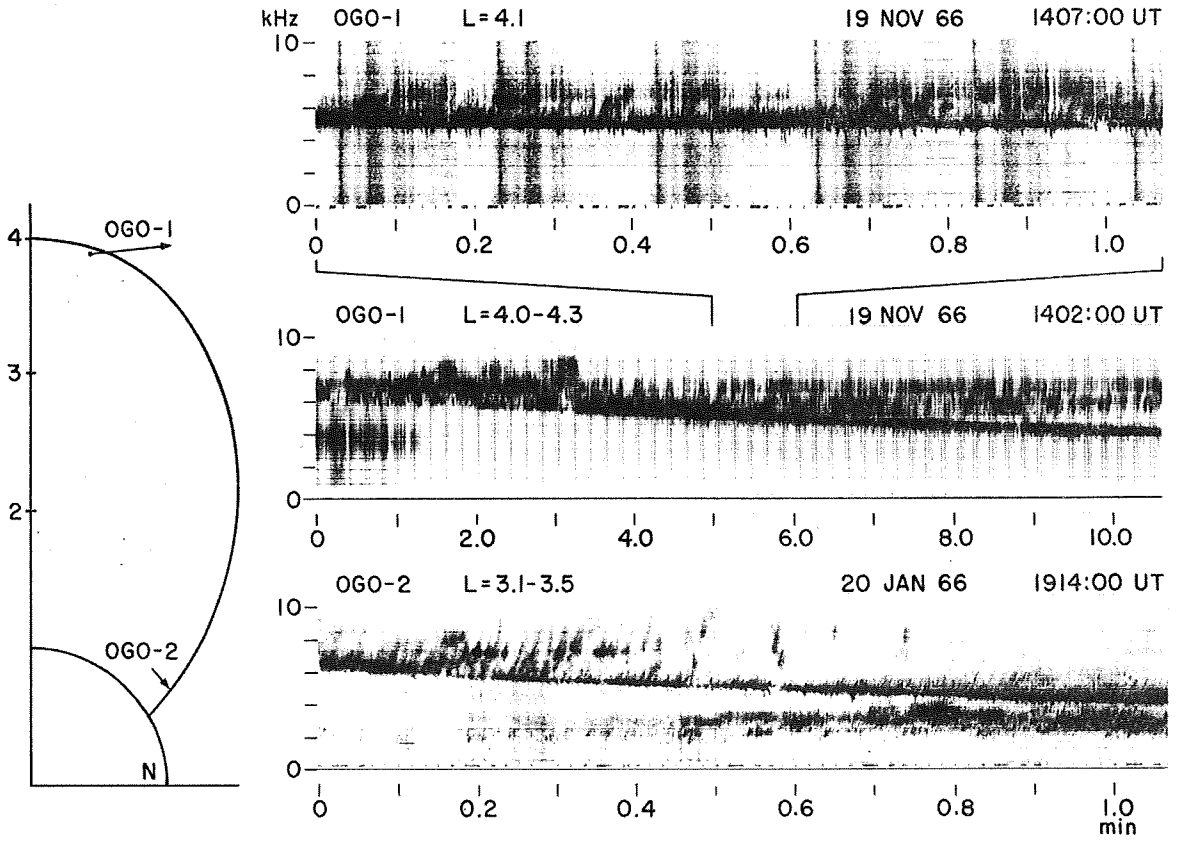
kHz
OGO-1
L=4.1
19 NOV 66
1407:00 UT
10
0
0
0.2
0.4
0.6
0.8
1.0
OGO-1
L=4.0-4.3
19 NOV 66
1402:00 UT
10
0
0
2.0
4.0
6.0
8.0
10.0
OGO-2
L=3.1-3.5
20 JAN 66
1914:00 UT
10
0
0
0.2
0.4
0.6
0.8
1.0
min
4
3
2
OGO-1
OGO-2
N

Figure 15

A.8

WHISTLER-MODE EMISSIONS ON THE OGO-1 SATELLITE (N. Dunckel and R. A. Helliwell, J. Geophys. Res., 74, 6371, 1969.)

This paper describes the spectrum and intensity of whistler-mode emissions detected by OGO 1 from perigee to apogee. One of its major contributions is comprehensive evidence that the upper-frequency end of the emission spectrum is controlled by conditions at the magnetic equator. This is the first experimental confirmation of its kind of an hypothesis often assumed in emission generation theories, that emissions are generated near the magnetic equator. Another important contribution is the first determination of the actual emission intensity in the vicinity of the equator. In Figure 16 these intensities in db above $10^{-3}\gamma\ (\mathrm{Hz})^{-1/2}$ are plotted in the equatorial plane in terms of LMT, the local mean time, and R_o, the geocentric distance in earth radii of the magnetic field line passing through the satellite. The darker shading represents areas of more intense emission activity. The major features of this figure are the two regions of intense activity near the noon meridian centered at $R_o = 4$ and 9, and the quiet nightside region commencing at midnight which abruptly becomes more active at 06 hours. The outer active region coincides with the region of strong fluxes of electrons identified by Vasyliunas [1968], from the M.I.T. modulated Faraday cup detectors on OGO 1 and OGO 3. The quiet nightside region appears to be a different regime, as discussed in item B.9 of this report.

With the aid of Figure 16, the broadband intensity of emissions at the equator averaged over all local mean times was estimated as a function of geocentric distance. These values may then be compared with

the estimates of emission intensity given by Kennel and Petschek [1966] assuming that the maximum radiation belt fluxes between $L = 4$ and $L = 7$ are limited by interaction with whistler-mode emissions. Since the intensity estimates all fall close to the measured values, these data verify that the radiation belts are indeed likely to be grossly affected by whistler-mode waves. Further research planned in this area includes a joint study with Vasyliunas to investigate in detail the relationship between emissions and low-energy electron fluxes.

Figure 16. Intensity of whistler-mode emissions mapped onto the equatorial plane versus local mean time in hours and R_o, the geocentric distance in the equatorial plane of the magnetic field line passing through the satellite. Each number represents the average of the peak intensities in each pass through that LMT-R_o block in db above $10^{-3}\gamma\ (Hz)^{-1/2}$. Values representing threshold levels are indicated by "<". Note two regions of intense emissions near the noon meridian and centered on $R_o = 4$ and 10. At local times from 22 to 06 hours, little or no noise is detected in the region beyond $R_o = 6$. Strong noise develops abruptly near 06 LMT.

References

Kennel, C. F. and H. E. Petschek, A limit on stably trapped particle fluxes, J. Geophys. Res., 71(1), 1-28, Jan. 1966.

Vasyliunas, V. M., Low-energy electrons on the day side of the magnetosphere, J. Geophys. Res., 73(23), 7519-7523, Dec. 1968.

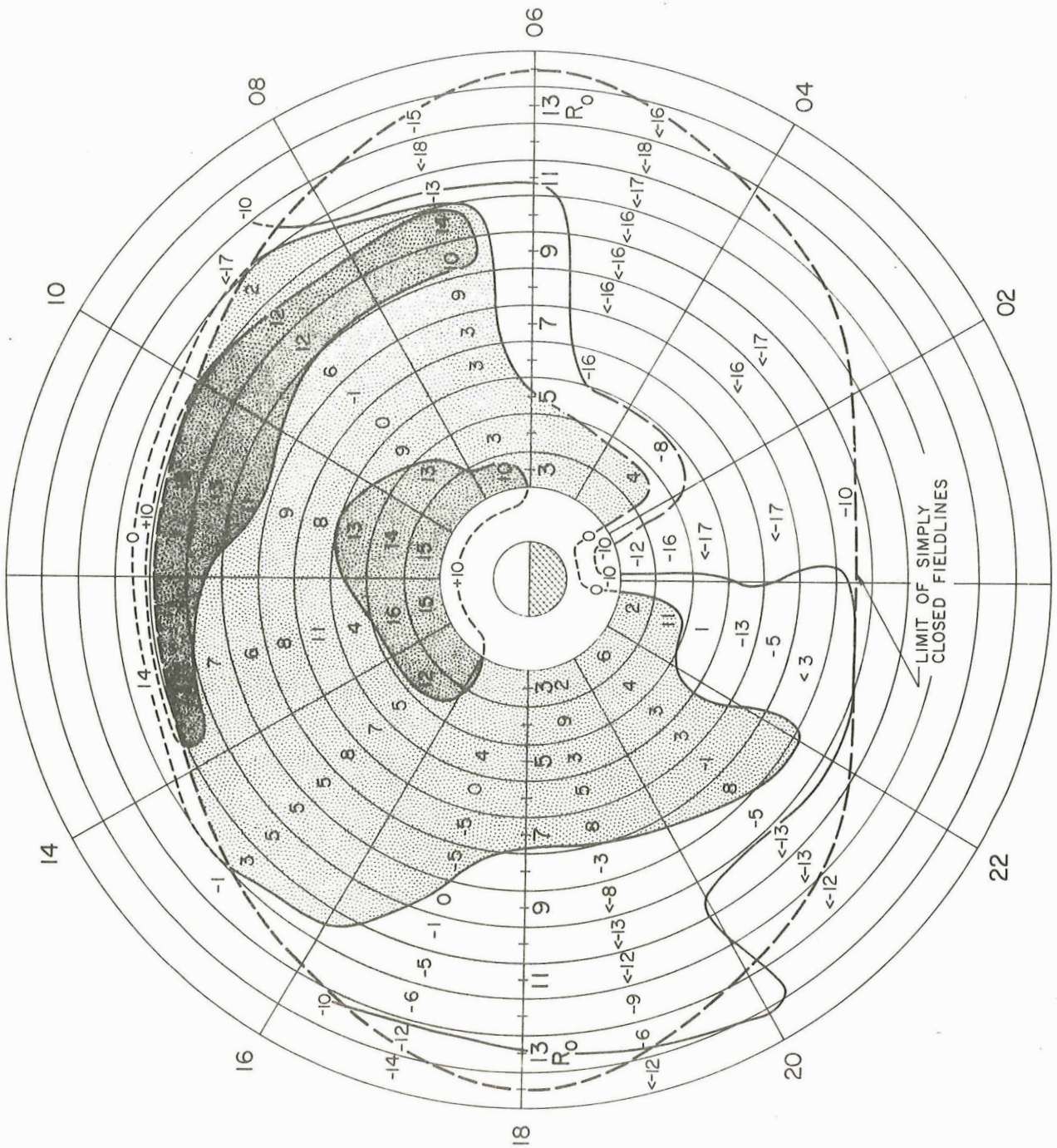
06
08
10
12
14
16
18
20
22
24
LMT
02
04
R_o
LIMIT OF SIMPLY
CLOSED FIELDLINES

Figure 16

A.9

OBSERVATION OF TWO NEW LOW-FREQUENCY NOISE PHENOMENA ON OGO 1
(N. Dunckel, B. Ficklin, L. H. Rorden and R. A. Helliwell, J. Geophys. Res., 75, March 1970.)

Two completely new types of low-frequency magnetic field noise have been detected by the VLF experiment on OGO 1. One type, called broadband noise, has a spectrum that covers the entire range of observations from 0.2 to 100 kHz. The other type, called highpass noise, has a spectrum that extends from a lower-cutoff frequency often near 40 kHz to at least 100 kHz. Both appear as bursts lasting of the order of 1 to 30 minutes. A remarkably high correlation has been found between the occurrence of these noises and magnetic conditions at the earth's surface in the polar regions. Not only does this correlation exist on an hour-to-hour basis, but also the commencement of these noises at the satellite has been found to occur within 2 min of the commencement on earth of polar substorm activity, even when the satellite is at geocentric distances of over 18 earth radii.

A plot of the occurrence of these noises in local mean time and L-value appears in Figure 17. It may be seen that the noises occur predominantly in the night hemisphere. Comparison with the whistler-mode emissions of Figure 16 shows that the two types of phenomena are spatially anti-correlated. A study on an event-to-event basis shows that this anti-correlation is practically perfect.

Figure 17. Broadband and highpass noise occurrence versus L in earth radii and local mean time in hours. Shading represents % occurrence. Crosses indicate that no data are available in that sector. Noises occur predominantly in the dark hemisphere approaching lowest L-shells near the midnight meridian.

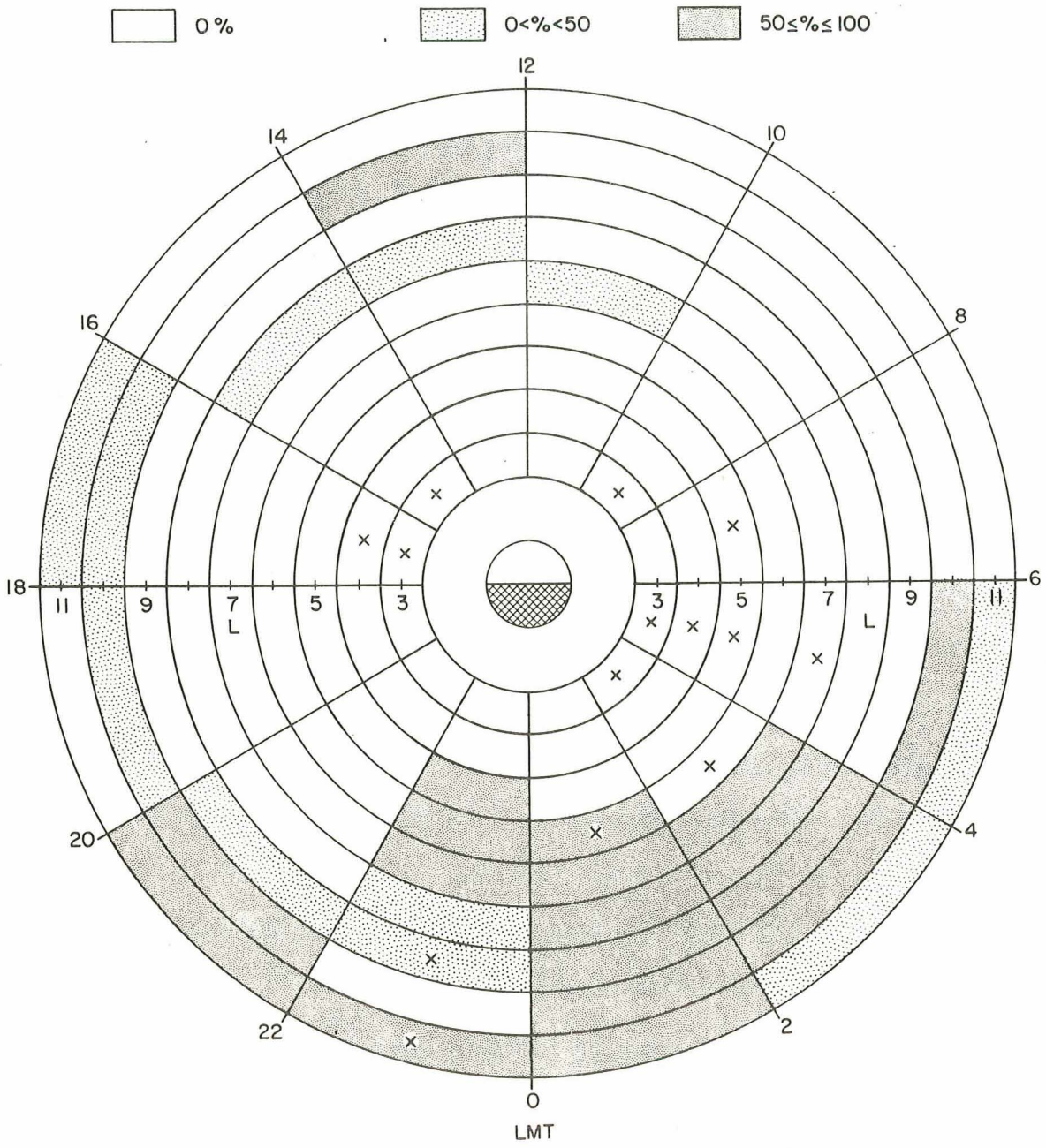

Figure 17

A.10

EMISSIONS OBSERVED BY OGO 3 BETWEEN THE MAGNETOPAUSE AND THE BOW SHOCK (J. J. Angerami, research in progress.)

Discrete emissions have been observed by the electric and magnetic sensors of the Stanford ELF receiver aboard OGO 3 in the transition region between the magnetopause and the bow shock. Both the occurrence and the frequency range of the emissions show a remarkable correlation with the intensity of the ambient magnetic field. The latter is measured by the onboard rubidium vapor magnetometer, and whose output appears as interference in the VLF channel.

The time-frequency spectrograms of Figure 18 illustrate the noise detected by the loop antenna of OGO 3 during the outbound magnetopause crossing on 14 September 1966. The top panel is a superposition of the data from the ELF (20 to $\sim$ 500 Hz) and VLF (.3 to 12.5 kHz) channels. The latter contains harmonics of one quarter the electron gyrofrequency (f_H), which are seen as horizontal lines in the beginning of the record, corresponding to a steady ambient magnetic field. After about 2239 UT, rapid fluctuations in the ambient magnetic field are shown by the gyrofrequency harmonic lines. Nearly coincident with this transition there is a change in the prevailing noise, from hiss to a band of discrete emissions. This noise is seen either on the top panel, which shows the center frequency of the band to be at $f_H/4$, or on the more expanded scale of the bottom panel, which contains the ELF channel data alone and therefore does not include the gyrofrequency harmonic lines.

Figure 19 illustrates discrete emissions observed by the electric field antenna on OGO 3 in the transition region. Discrete emissions tend to predominate over hiss when the ambient magnetic field shows a

sharp dip, and have been seen in the frequency range from 1/4 to 5/8 of the local electron gyrofrequency.

Further studies of this phenomenon are in progress.

Figure 18. Frequency-time spectra to illustrate a change in the ELF noise activity across the magnetopause. In the top panel the data from both the ELF (20 to $\sim$ 500 Hz) and VLF (.3 to 12.5 kHz) channels are superimposed. The latter includes harmonics of one quarter the electron gyrofrequency, indicated by the scale on the right. The ELF channel contains no magnetometer output and the corresponding noise data are shown alone in the bottom panel. The change in ambient magnetic field from constant to rapidly varying (top panel) is accompanind by a change in the noise activity from hiss to a band of discrete emissions (bottom panel). As shown by the superposition in the first panel, this band centers at one quarter of the local gyrofrequency.

Figure 19. Frequency-time spectrum illustrating the appearance of discrete emissions at dips of the magnetic field in the transition region. The low frequency end of the record, representing data from the ELF channel, shows a band of hiss interrupted by the occurrence of two strong emissions, coincident with abrupt decreases in the local gyrofrequency f_H (scale on the right).

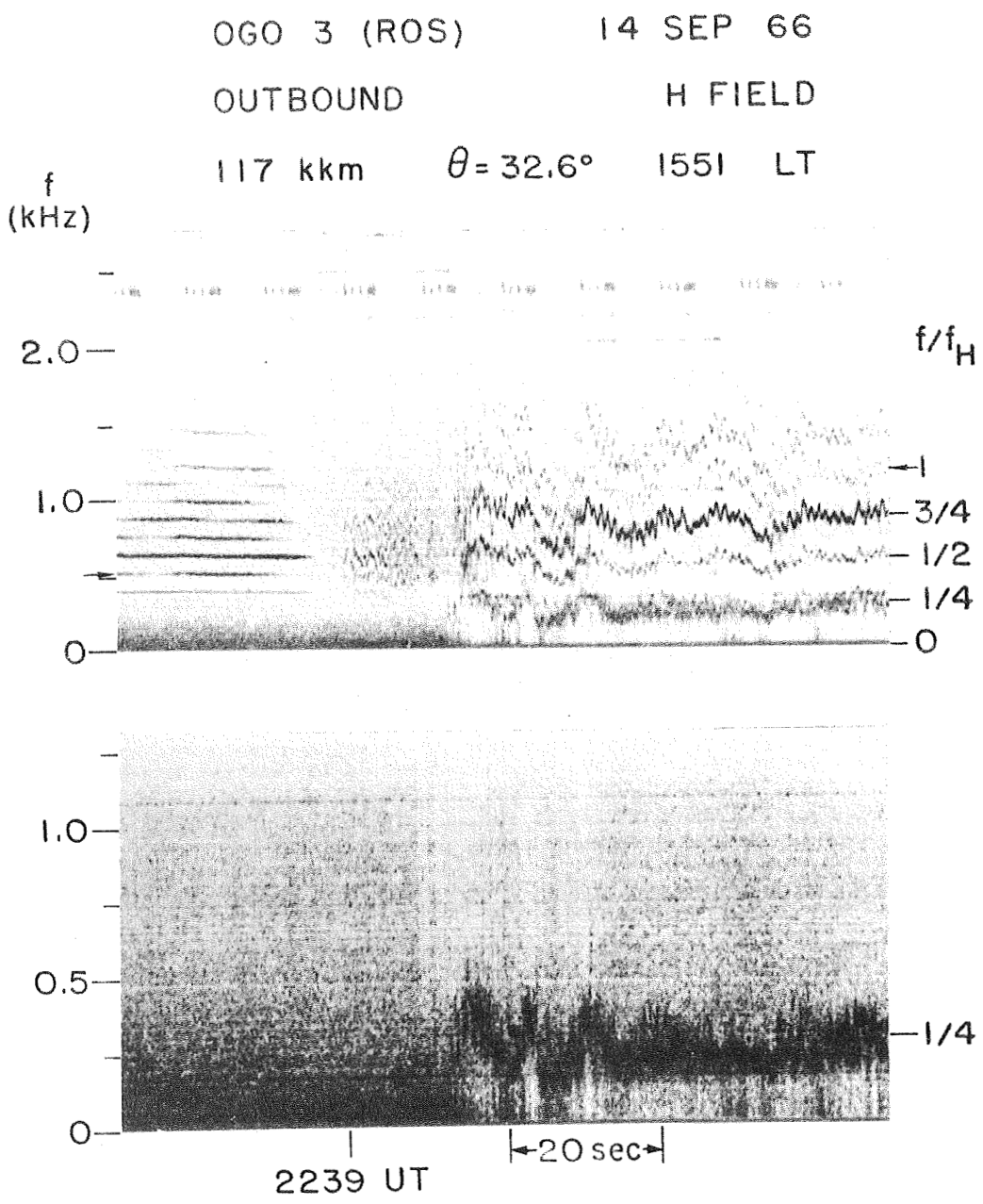
OGO 3 (ROS) 14 SEP 66
OUTBOUND H FIELD
117 kkm θ = 32.6° 1551 LT
f (kHz)
2.0
1.0
0
f/f_H
1
3/4
1/2
1/4
0
1.0
0.5
0
1/4
20 sec
2239 UT

Figure 18

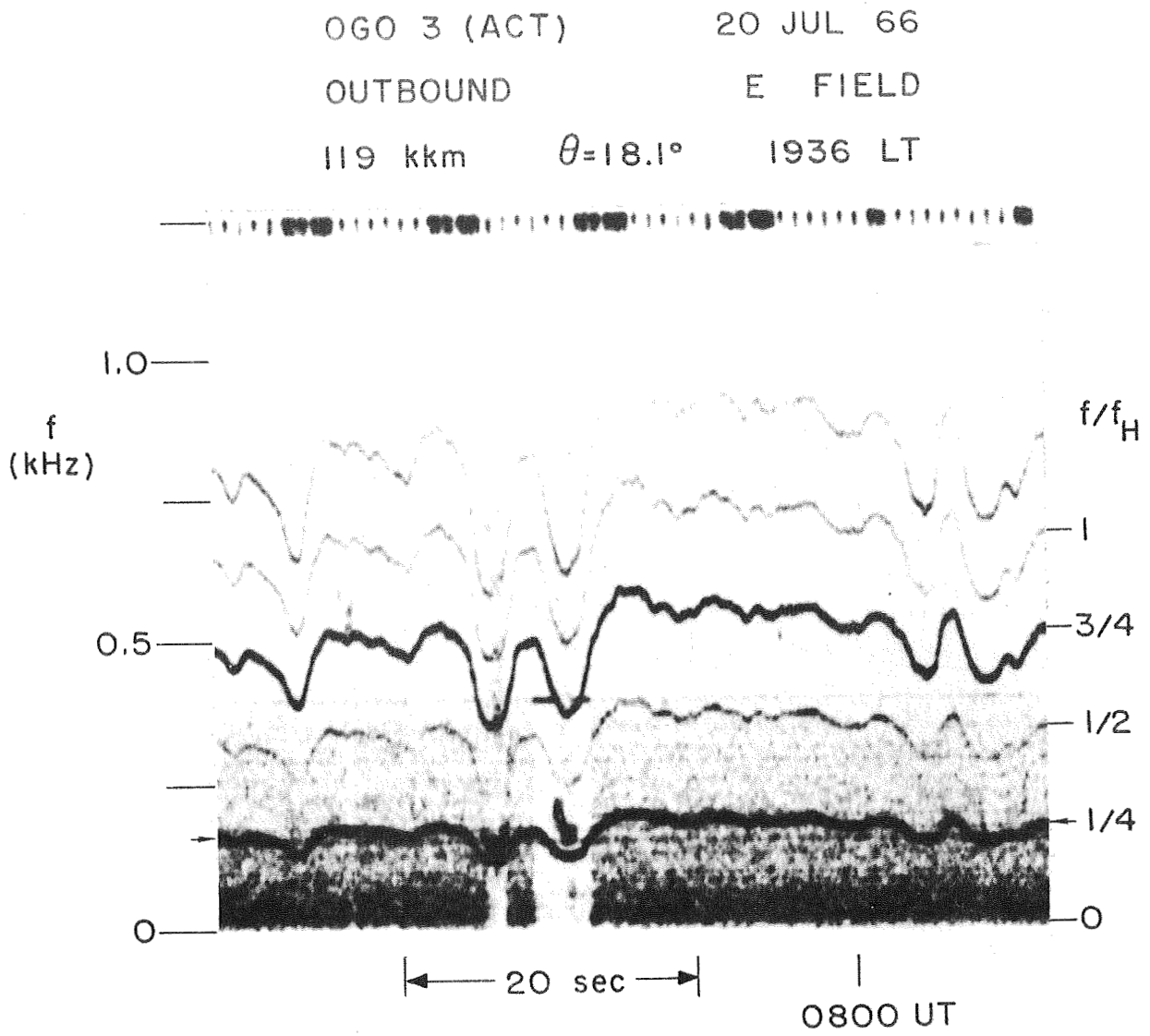
OGO 3 (ACT)
20 JUL 66
OUTBOUND
E FIELD
119 kkm
θ=18.1°
1936 LT
1.0
f
(kHz)
0.5
0
f/f_H
1
3/4
1/2
1/4
0
20 sec
0800 UT

Figure 19

A.11

MULTI-EXPERIMENT DETECTION OF THE PLASMAPAUSE FROM OGO 1 AND OGO 3 AND ANTARCTIC GROUND STATIONS (D. L. Carpenter, C. G. Park, H. A.Taylor, Jr. and H. C. Brinton, J. Geophys. Res., 74, 1837, 1969.)

As more is learned of the plasmapause it has become evident that the plasmapause radius exhibits relatively large variations with time, magnetic activity and longitude. During the recovery phase of magnetic storms the radius may appear to be multi-valued, with plasmapause "effects" appearing on several different magnetic shells at a given magnetic meridian. Because of these complexities it is important to compare measurements by various techniques and also to inter-compare measurements made simultaneously with various longitudinal spacings. Some such comparisons have been made of data from the GSFC ion mass spectrometers and the Stanford/SRI VLF receivers on the OGO-1 and OGO-3 satellites. Comparisons have also been made of the mass spectrometer data from an OGO satellite and simultaneous whistler recordings on the ground near the prime geomagnetic meridian. In the satellite VLF data the plasmapause crossings are identified by abrupt changes in observed whistler and VLF noise activity and by noise bands of limited duration. In one case from OGO 1 and one from OGO 3, plasmapause crossings were detected by both the VLF and ion experiments within less than 0.1 R_E in L value. In eight cases of OGO-1 ion data and simultaneous ground whistler data spaced 1 to 12 hours from OGO 1 in local time, good agreement was found between the plasmapause positions measured from the two experiments. The comparisons provide new verification of the essentially worldwide extent of the plasmapause and also verify previous indications that the radius of the plasmapause is frequently about

constant over large local-time sectors in the range 0-18 LT.

Figure 20. Comparison of simultaneous VLF and ion mass spectrometer data on a plasmapause crossing during the OGO-3 outbound pass of July 5, 1966. The satellite orbit is shown in a geomagnetic meridian projection. A pair of arrows along the orbit indicates the position of the plasmapause as detected in the ion data. The corresponding time interval is shown by arrows on the ion and VLF records. The VLF data being in the top panel and continue outbound toward the plasmapause in the bottom panel. Horizontal lines on the records are of instrumental origin. The VLF signal descending in frequency after 12h 38m 30s is interference from the onboard magnetometer.

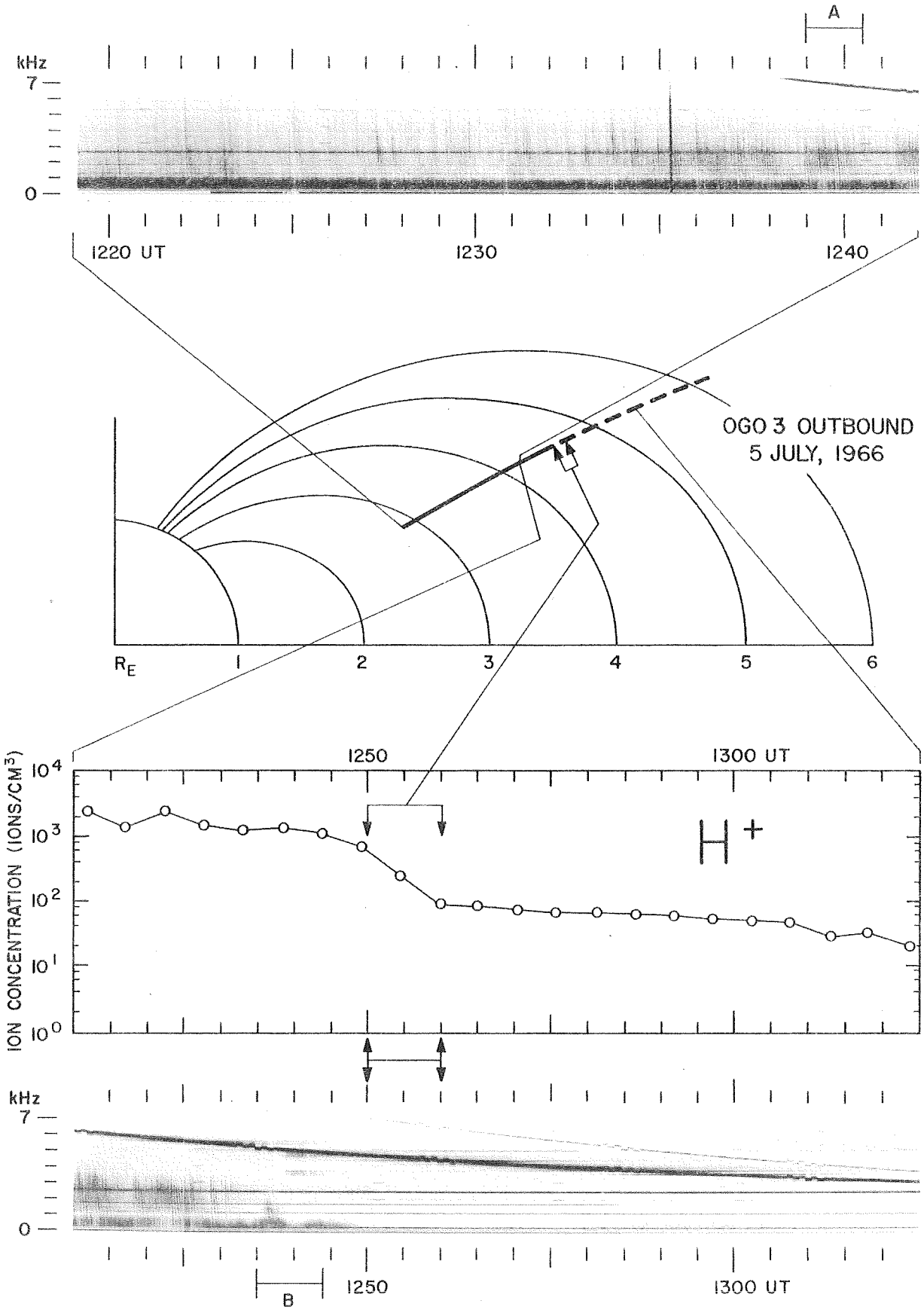
A
kHz
7
0
1220 UT
1230
1240
OGO 3 OUTBOUND
5 JULY, 1966
R_E
1
2
3
4
5
6
1250
1300 UT
ION CONCENTRATION (IONS/CM^3)
10^4
10^3
10^2
10^1
10^0
H^+
kHz
7
0
B
1250
1300 UT

Figure 20

A.12

OBSERVATIONS OF PLASMAPAUSE CROSSINGS MADE WITH HIGH TIME RESOLUTION (N. Dunckel, research in progress.)

On many OGO-1 passes a direct indication of the plasmapause is obtained. The intensity of the inverter signals (at multiples of 2.461 kHz) in the frequency range 40-100 kHz appears perhaps 8 db stronger inside the plasmapause than outside. For instance, on an outbound pass of OGO 1 on May 8, 1965, the inverter levels prior to 1147 UT were all high. At first the levels near 100 kHz dropped, then those at progressively lower frequencies. Fifty-one seconds after the initial variation at 100 kHz, the inverter intensities down to 40 kHz had dropped and no further changes appeared. The location of the satellite at 1146 UT was such that $L = 4.7$, magnetic latitude = 30^{o}, LMT = 23 hours, and f_H = 28 kHz. The observation of the plasmapause on the same satellite by H. Taylor at 1146 UT (personal communication) confirms that the satellite was crossing the plasmapause at that time. Although the phenomenon is not fully understood, it appears that the conditions for the inverters being high may be that these frequencies fall in the non-propagating region given by $f_p/f \gtrsim 1$, $f_H/f < 1$. In this case the plasma frequency is approximately the frequency above which the inverters are depressed and below which they are enhanced. The abrupt decrease of the plasma frequency in the vicinity of the plasmapause then causes the observed effect. According to this interpretation, the satellite moved only $L = 0.06$ earth radii while the plasma frequency dropped approximately from 100 to 40 kHz. Thus, the high time resolution of the present experiment (one sweep each 2.3 seconds at high bit rate) permits a more accurate description of the abrupt changes of plasma frequency near the plasmapause than heretofore possible.

A.13

OBSERVATIONS OF WHISTLER-MODE SIGNALS IN THE OGO SATELLITES FROM VLF GROUND STATION TRANSMITTERS (R. L. Heyborne, PhD Dissertation, SEL-66-094, Stanford University, Stanford, Calif., Nov. 1966.)

The field intensities from VLF transmitters (in the vicinity of 20 kHz) as observed from OGO 1 and OGO 2 were surveyed and compared with theoretical predictions. The new observations include a latitudinal cutoff, antipodal enhancements, an equatorial reduction of intensity, unexpected fading patterns, and possible observation of ducted signals. The latter two phenomena are illustrated in Figures 21 and 22. The latitudinal cutoff is discussed in Appendix A.1 of the OGO 2 and OGO 4 report.

Figure 21. Examples of burst-like signals from station NPG (18.6 kHz) received on OGO 1. Nonducted signals, which should be fairly continuous in nature, apparently were not reaching the satellite position. The burst-like character of the signals suggests that they resulted from ducted propagation and the temporary intersection of the satellite with various ducts of enhanced ionization.

Figure 22. Examples of deep and rapid fading of signals from NPG as observed from OGO 2. This fading has not yet been explained. One possibility is the interference of from two to four wave modes excited from one wave upon encountering field aligned irregularities.

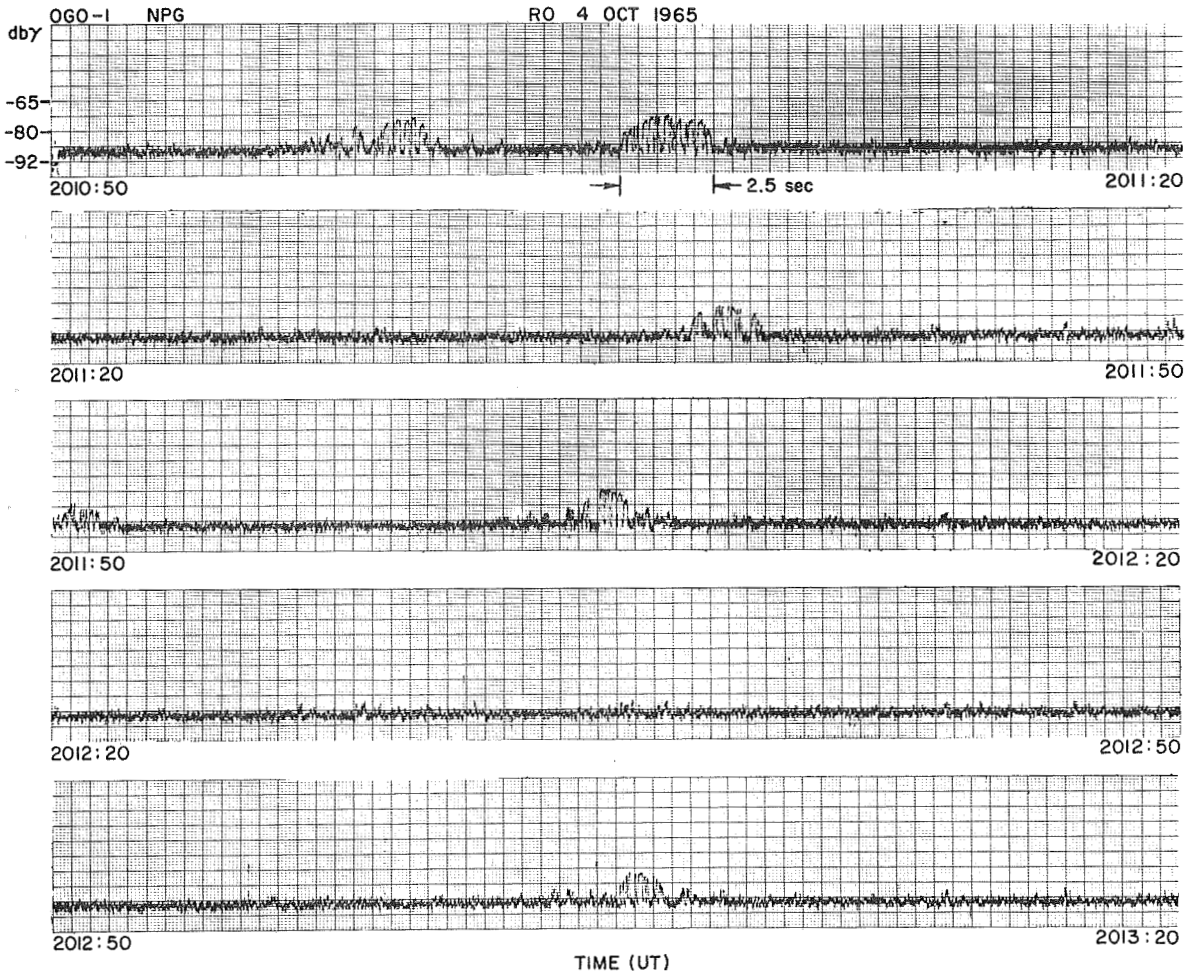
OGO-1 NPG
RO 4 OCT 1965
dbγ
-65
-80
-92
2010:50
2.5 sec
2011:20
2011:20
2011:50
2011:50
2012:20
2012:20
2012:50
2012:50
2013:20
TIME (UT)

Figure 21

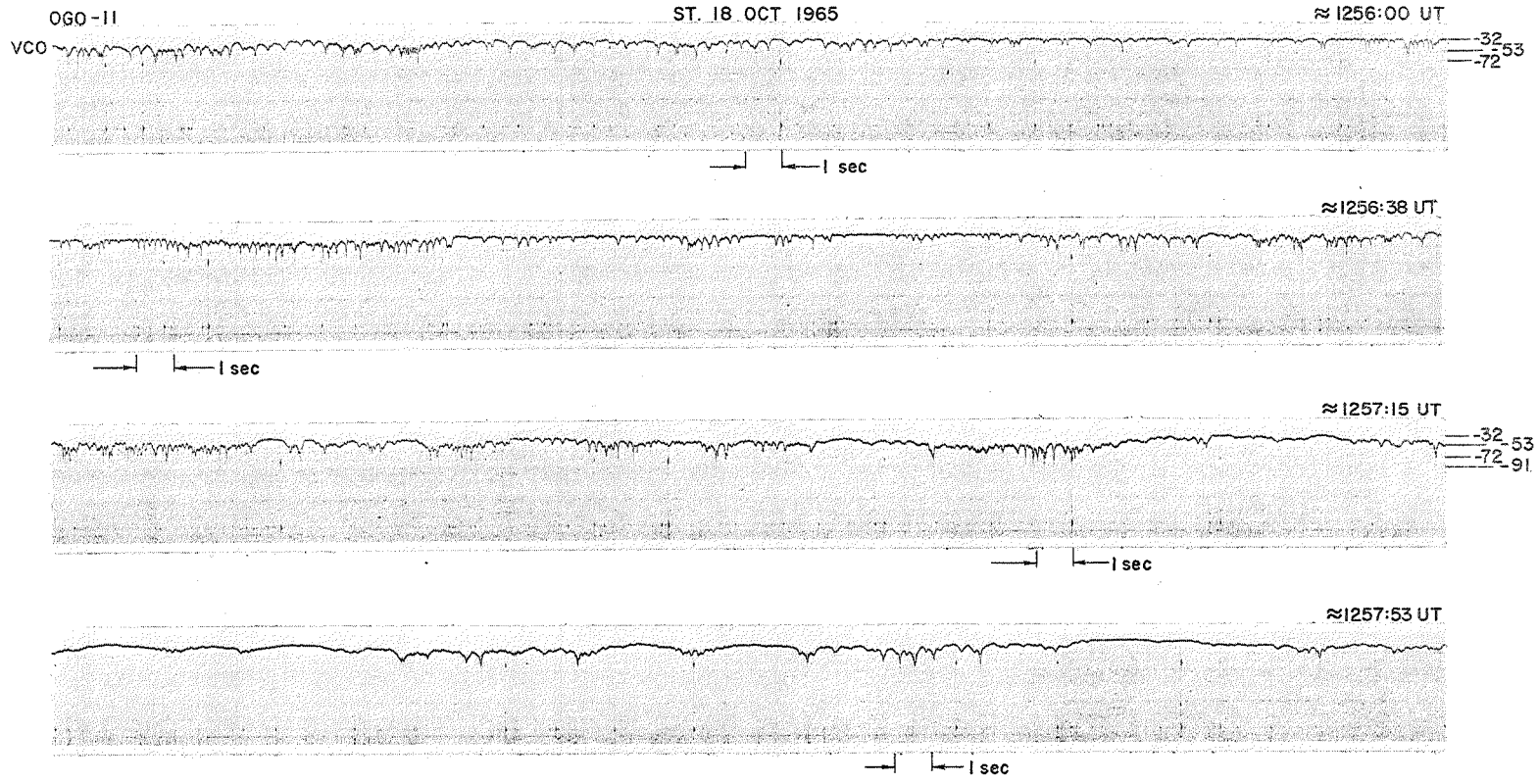
OGO-II
ST. 18 OCT 1965
≈1256:00 UT
VCO
-32
-53
-72
1 sec
≈1256:38 UT
1 sec
≈1257:15 UT
-32
-53
-72
-91
1 sec
≈1257:53 UT
1 sec

Figure 22

A.14

SUPER-GYROFREQUENCY WHISTLERS (R. L. Smith, research in progress.)

An extremely rare type of whistler, observed on OGO 3 during the inbound pass of 21 January 1967, is shown in the frequency-time spectra of Figure 23. The satellite was located 9.8 degrees south of the geomagnetic equator at an L-value of 5.24. The local time at the subsatellite point was 1038. The top panels in the figure show three of the best examples of the phenomenon, referred to as a "super-gyrofrequency whistler" (SG whistler) and consisting of descending tones from approximately 10 kHz to 7.5 kHz. These spectra also show horizontal lines at harmonics of $f_H/4$, one quarter the local electron gyrofrequency, measured by the onboard rubidium-vapor magnetometer. The corresponding scales at the right indicate that the three SG whistlers are clearly above f_H, giving rise to their designation.

The SG whistlers reported here are the only examples known to date. In this pass of OGO 3 nine events were observed over a three-minute time interval, between L-values of 5.32 and 5.23 and dipole latitudes of 9.4^{o}S and 9.8^{o}S. A discrete rising emission, starting at about 2 kHz, preceded every whistler event by a constant time lapse of about half a second, as shown in the figure. Similar emissions - but not the SG whistlers - were also observed on the ground at Byrd Station, Antarctica, near the southern foot of the field line passing through the satellite. In the conjugate region, however, only sferics were observed, as shown by the Great Whale River (GWR) record in the bottom panel of Figure 23. It was therefore concluded that the SG whistlers originated in the northern hemisphere. This conclusion was further corroborated by the correlation between the sferics and the rising emissions which, as shown in the two

bottom panels, enabled the identification of the source of the SG whistler.

Preliminary analysis of the above data has indicated that the SG whistler may result from propagation in the extraordinary mode above the plasma frequency ("z-mode"). At present this explanation is not considered satisfactory because of difficulties, including the coupling to the left hand mode through the ionosphere, an excessive observed time delay, and a plasma frequency at the satellite that is lower than consistent with the delay for the emissions.

Further investigation of this unique phenomenon is in progress.

Figure 23. The three top panels are frequency-time spectra of OGO-3 data illustrating super-gyrofrequency (SG) whistlers. The bottom panel is a simultaneous ground record made at Great Whale River (GWR), near the northern foot of the field line passing through the satellite. The SG whistlers are falling tones approaching asymptotically a frequency of about 7 kHz, which, as shown by the scale on the right, is greater than the local gyrofrequency. Rising tones starting near 2 kHz precede the SG whistlers by about 0.5 sec. The vertical arrows at the bottom of the panels indicate the time of occurrence of the sferics producing the rising emissions and the associated SG whistlers. As shown in the bottom panel, the sources were identified in the northern hemisphere (see text).

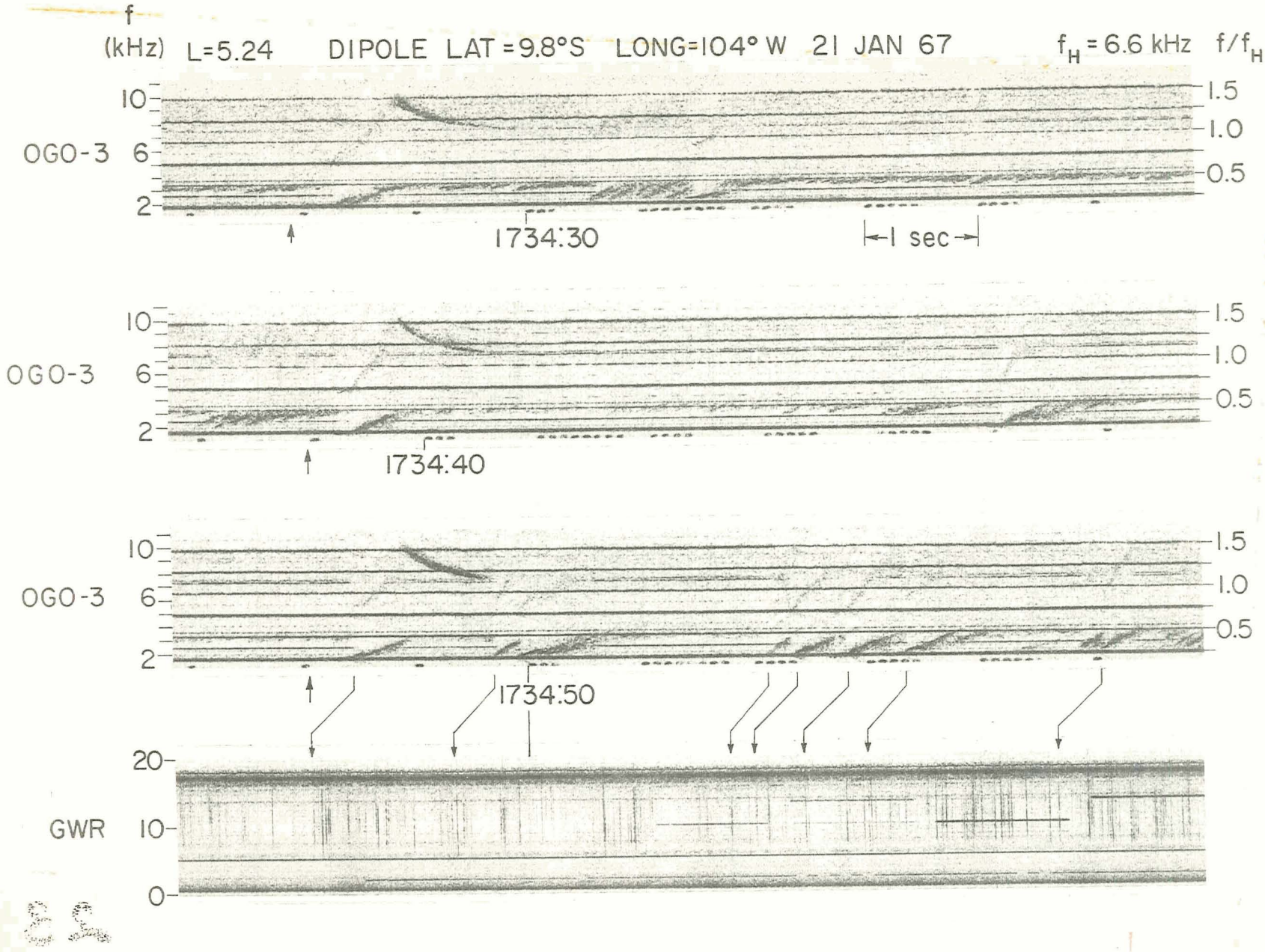
f
(kHz)
L=5.24
DIPOLE LAT=9.8°S LONG=104° W 21 JAN 67
f_H = 6.6 kHz
f/f_H
OGO-3
10
6
2
1.5
1.0
0.5
1734:30
1 sec
OGO-3
1734:40
OGO-3
1734:50
GWR
20
10
0

Figure 23

VI. APPENDIX B

Included in Appendix B are the following illustrations: a block diagram of the experiment package and calibration curves of the receivers.

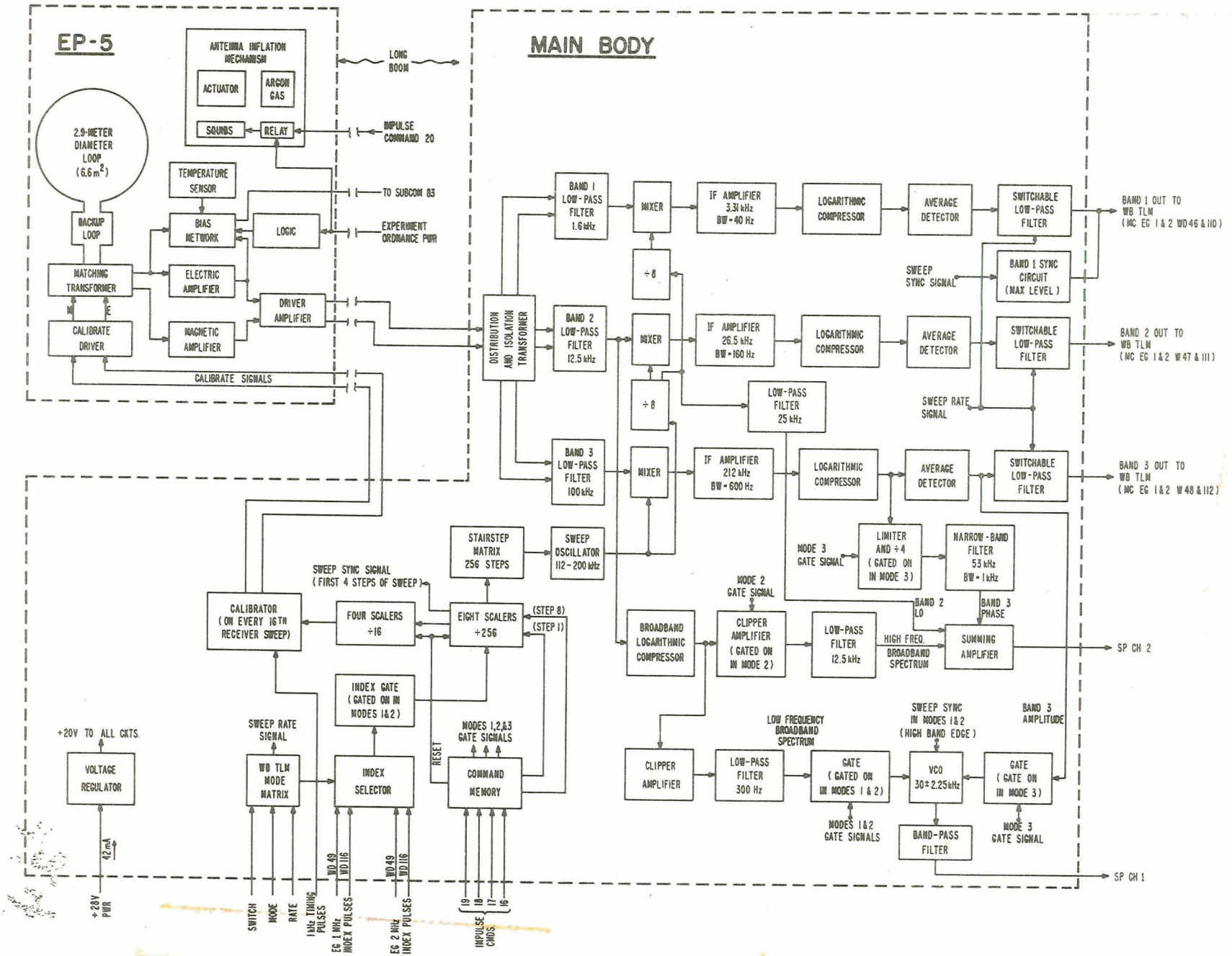

Figure 24. Block diagram of EXP B 17 in OGO 3. EXP A 17 in OGO 1 is similar but does not contain the electric antenna nor the ELF receiver (see section II.B).

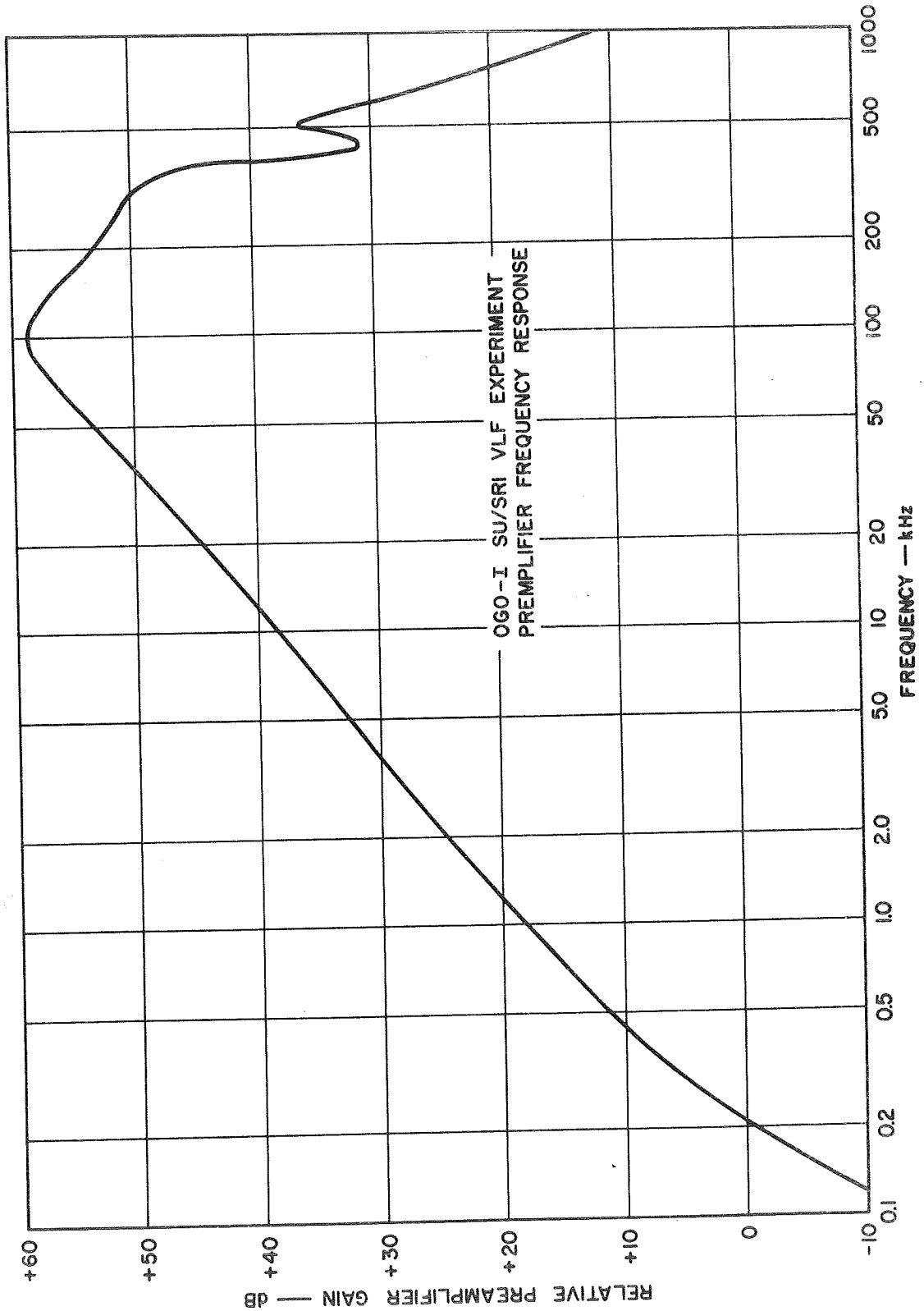

Figure 25. Relative frequency response of preamplifier (OGO 1).

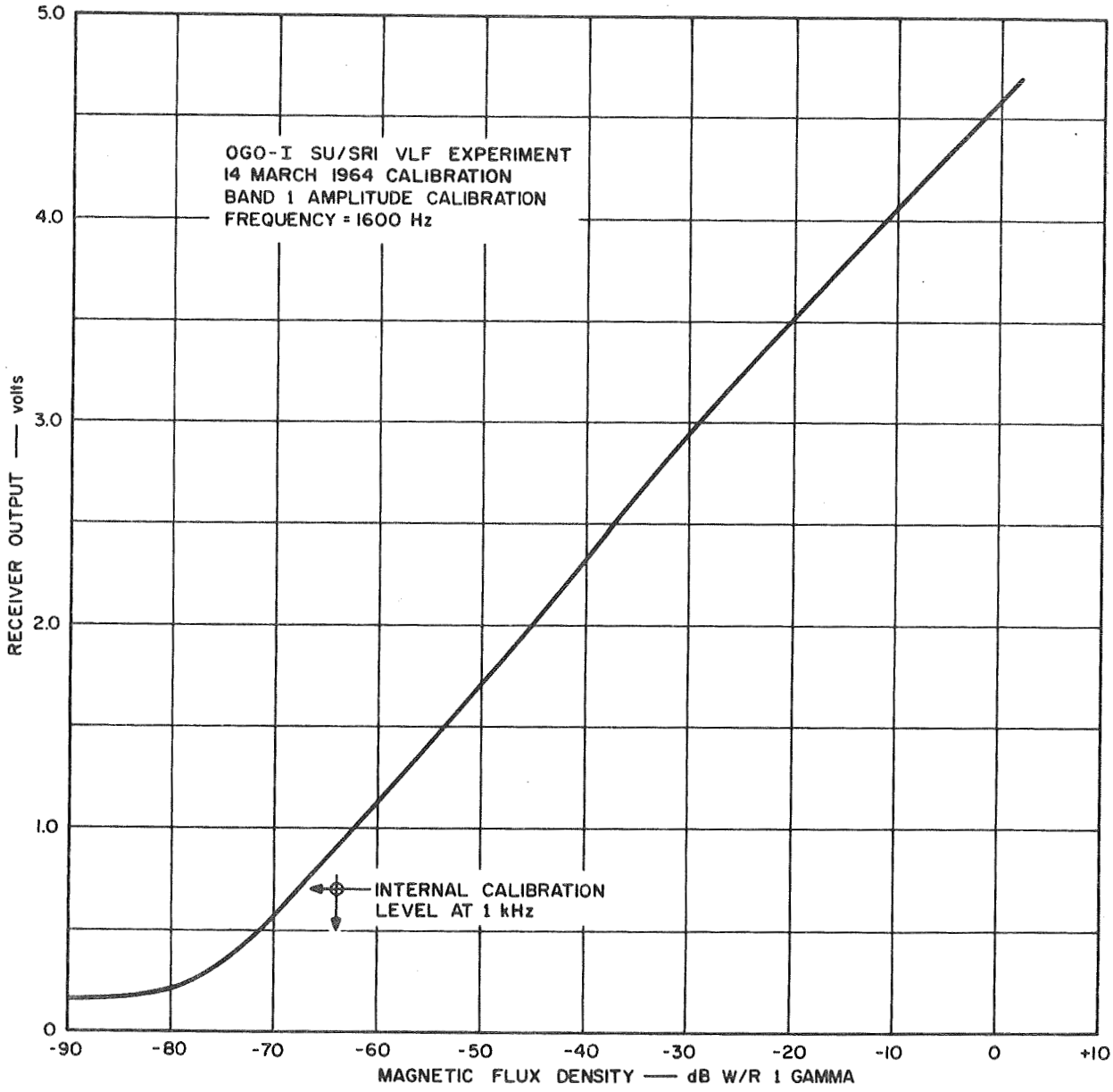

Figure 26. OGO-1 calibration of Band 1 at 1600 Hz. Use Figure 25 for calibration at other frequencies. Note the logarithmic response, due to the log compressors of Figure 24.

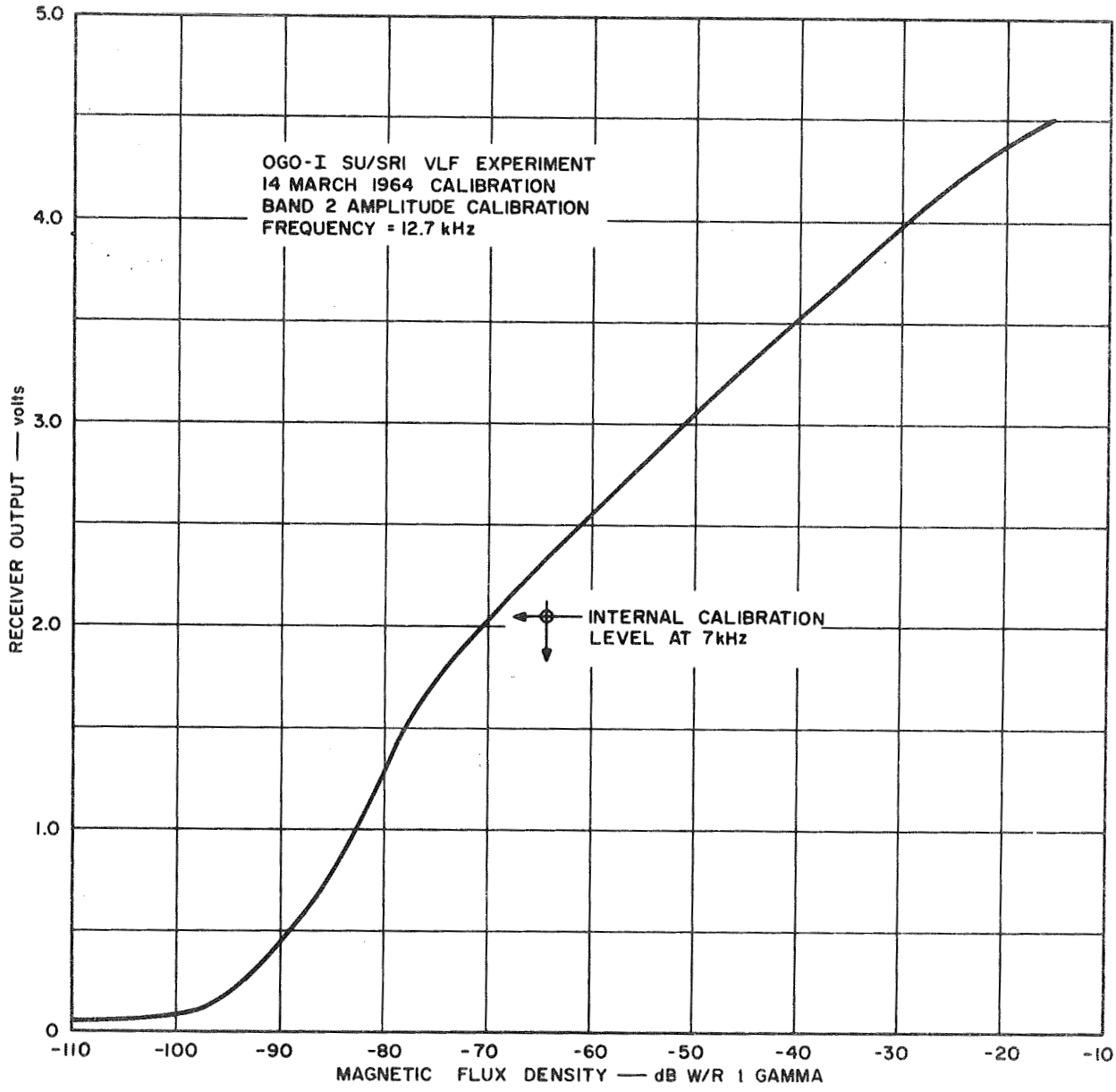

Figure 27. OGO-1 calibration of Band 2 at 12.7 kHz. Use Figure 25 for calibration at other frequencies. Note the logarithmic response, due to the log compressors of Figure 24.

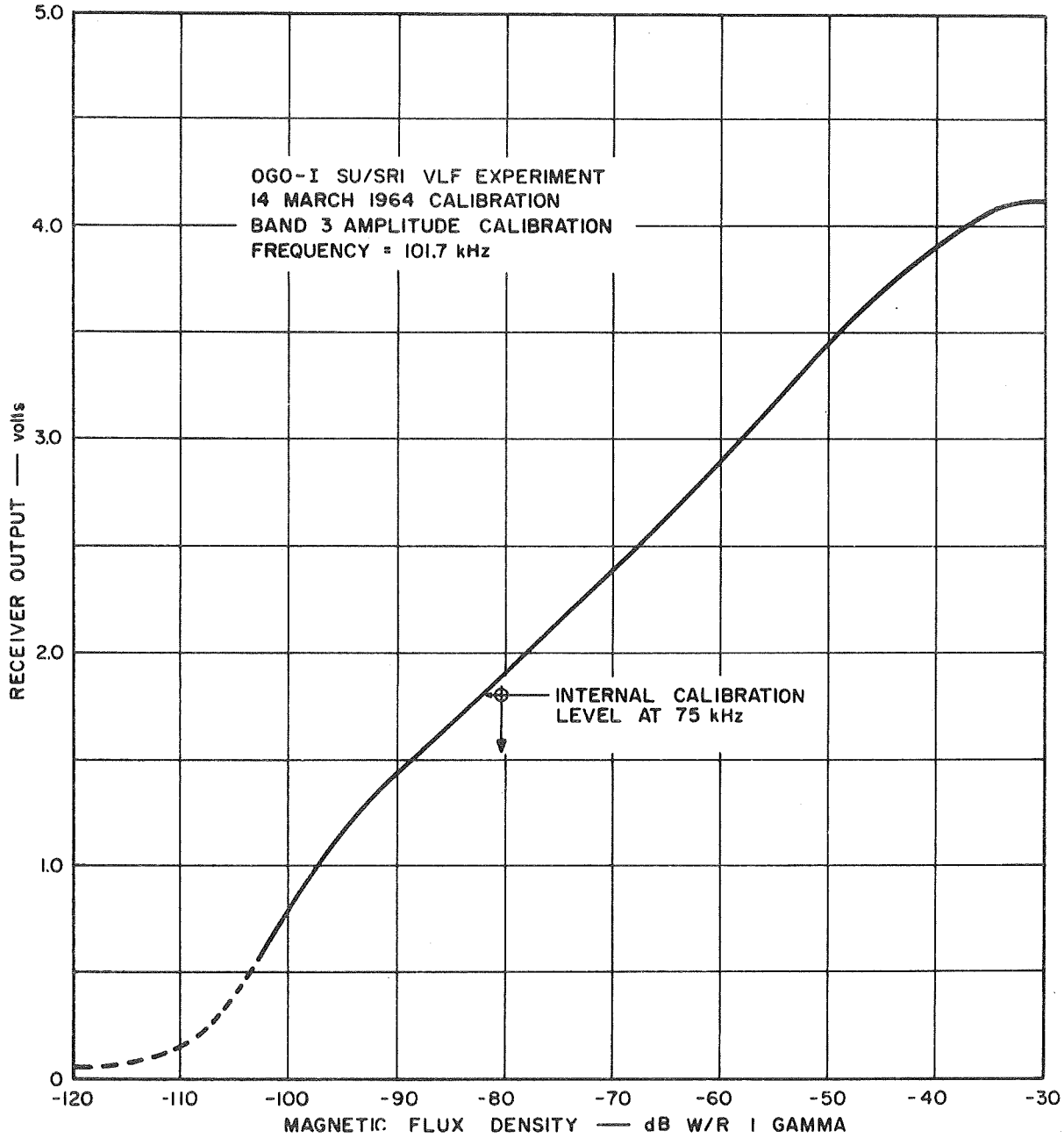

Figure 28. OGO-1 calibration of Band 3 at 101.7 kHz. Use Figure 25 for calibration at other frequencies. Note the logarithmic response, due to the log compressors of Figure 24.

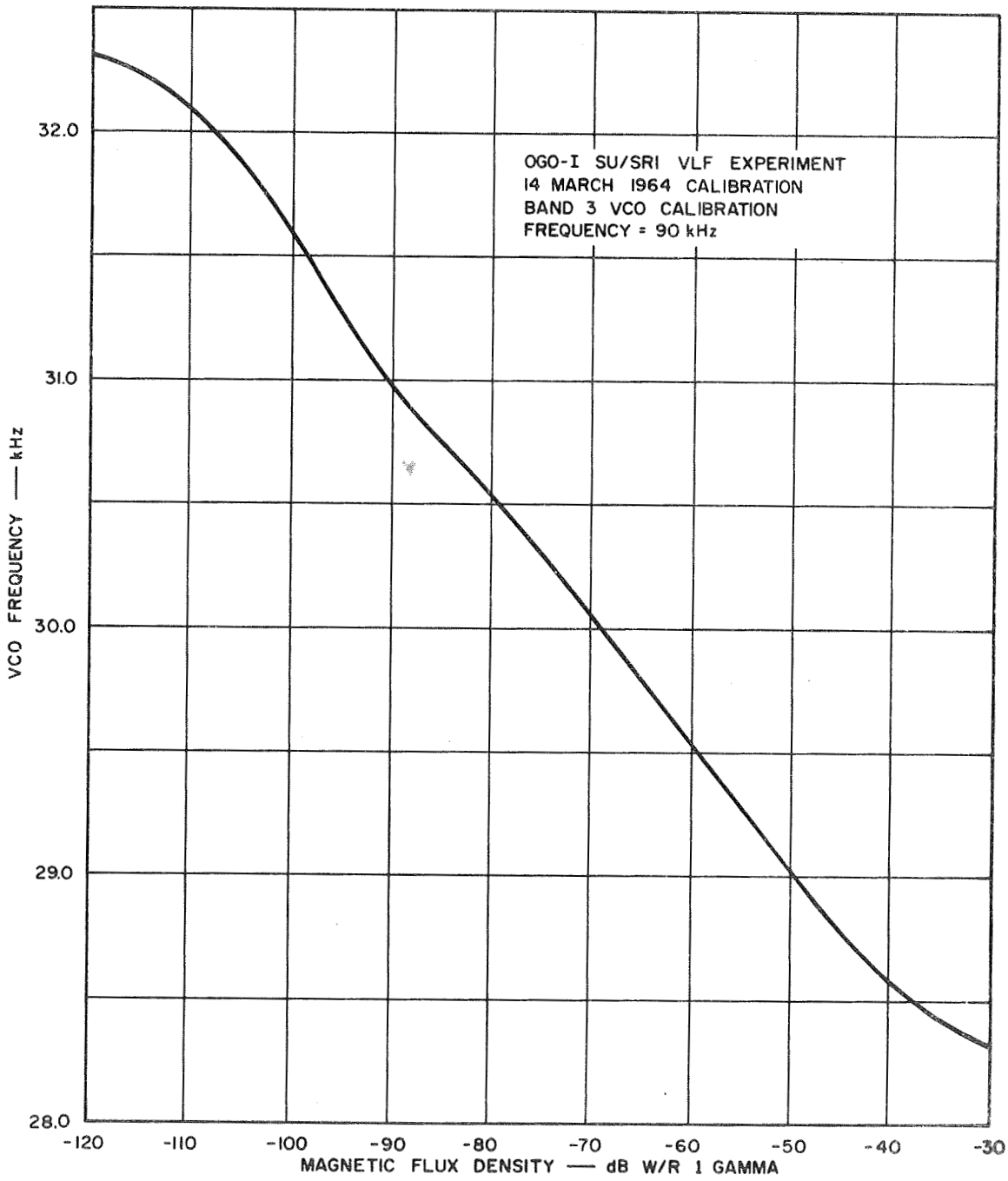

Figure 29. OGO-1 calibration of voltage-controlled oscillator (VCO) for Band 3 tuned to 90 kHz (mode 3). Use Figure 25 for calibration at other frequencies.

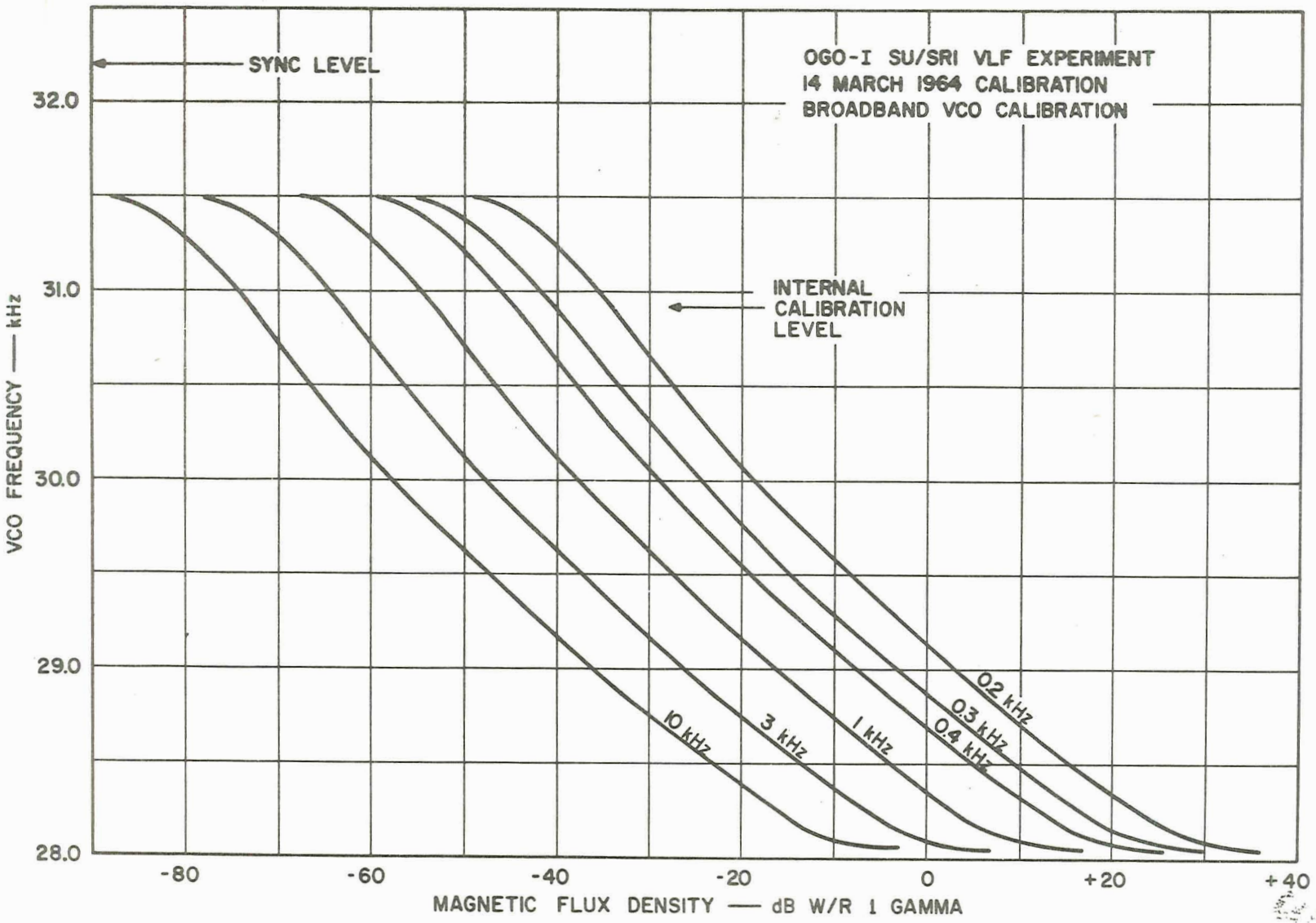

Figure 30. OGO-1 calibration of voltage-controlled oscillator (VCO) for six different frequencies applied to the broadband receiver (modes 1 or 2).

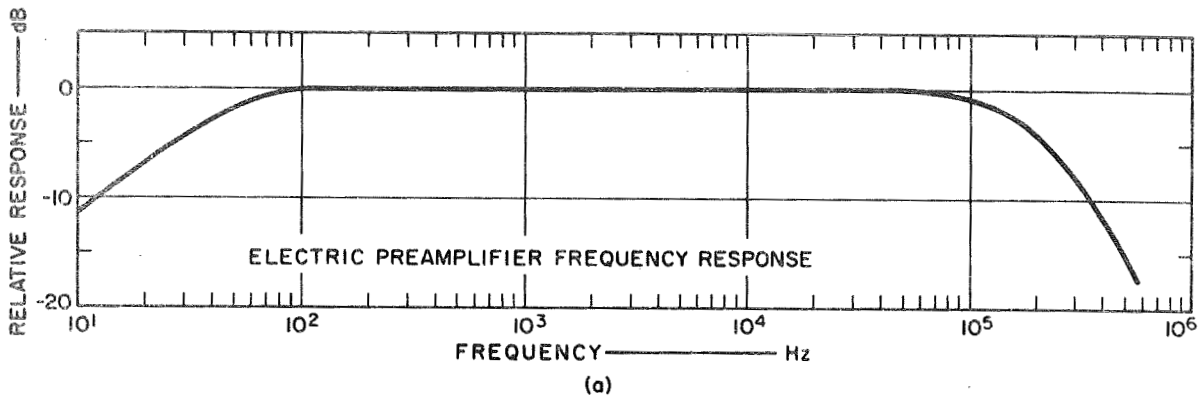

(a)

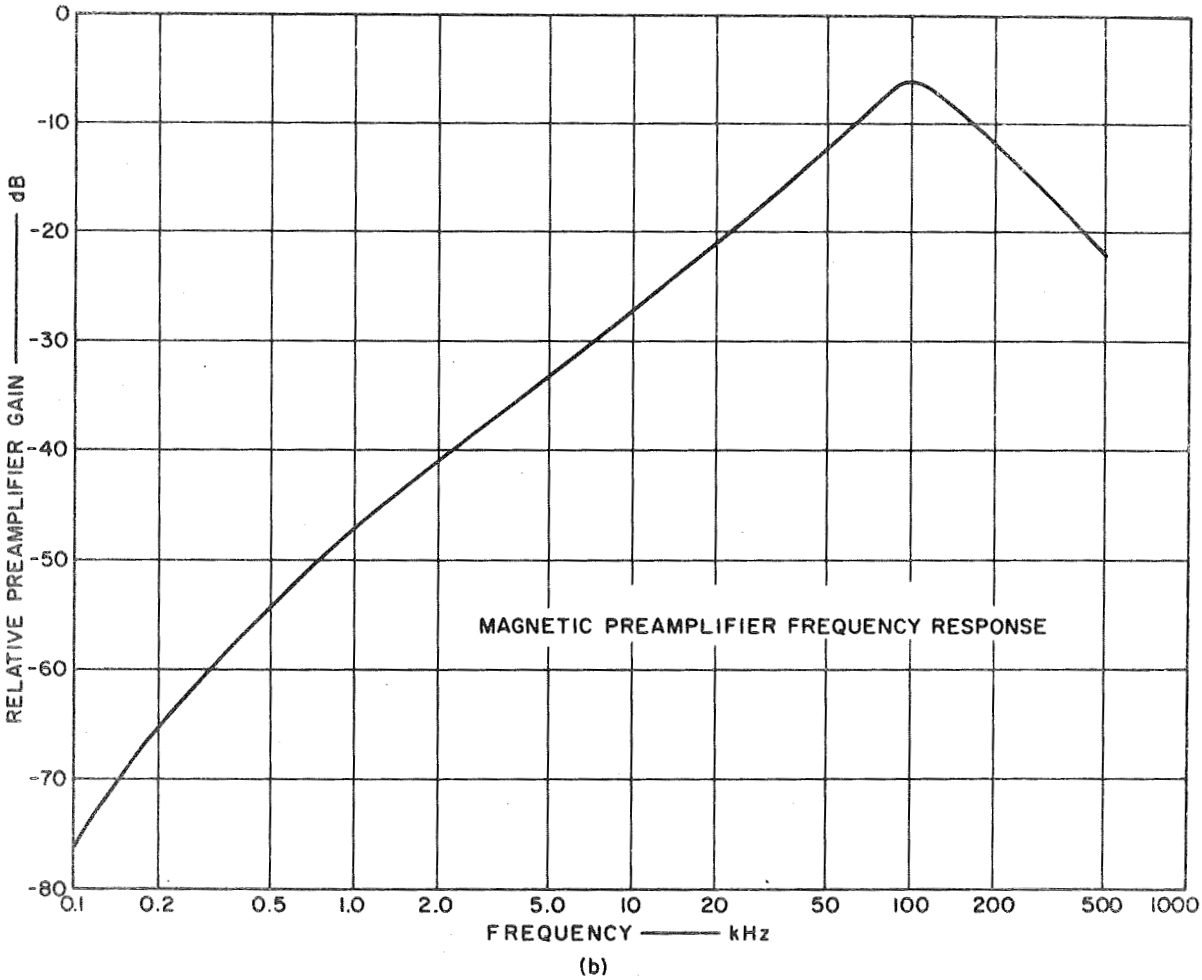

(b)

Figure 31. Relative frequency responses of the electric (top) and magnetic (bottom) preamplifiers of EXP 17 in OGO 3.

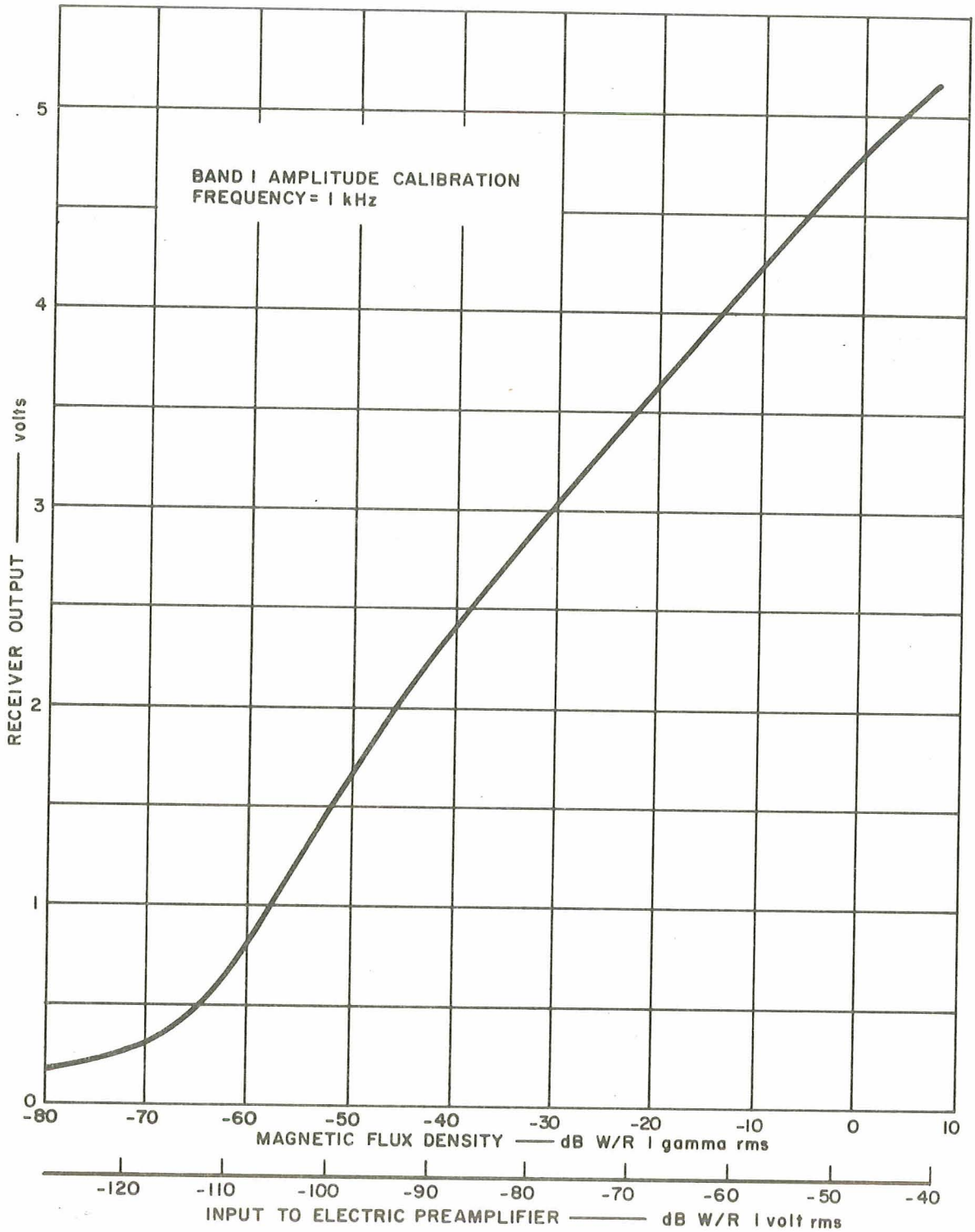

Figure 32. OGO-3 calibration of Band-1 receiver at 1 kHz. Use Figure 31 for calibration at other frequencies. Note the logarithmic response due to the log compressors of Figure 24.

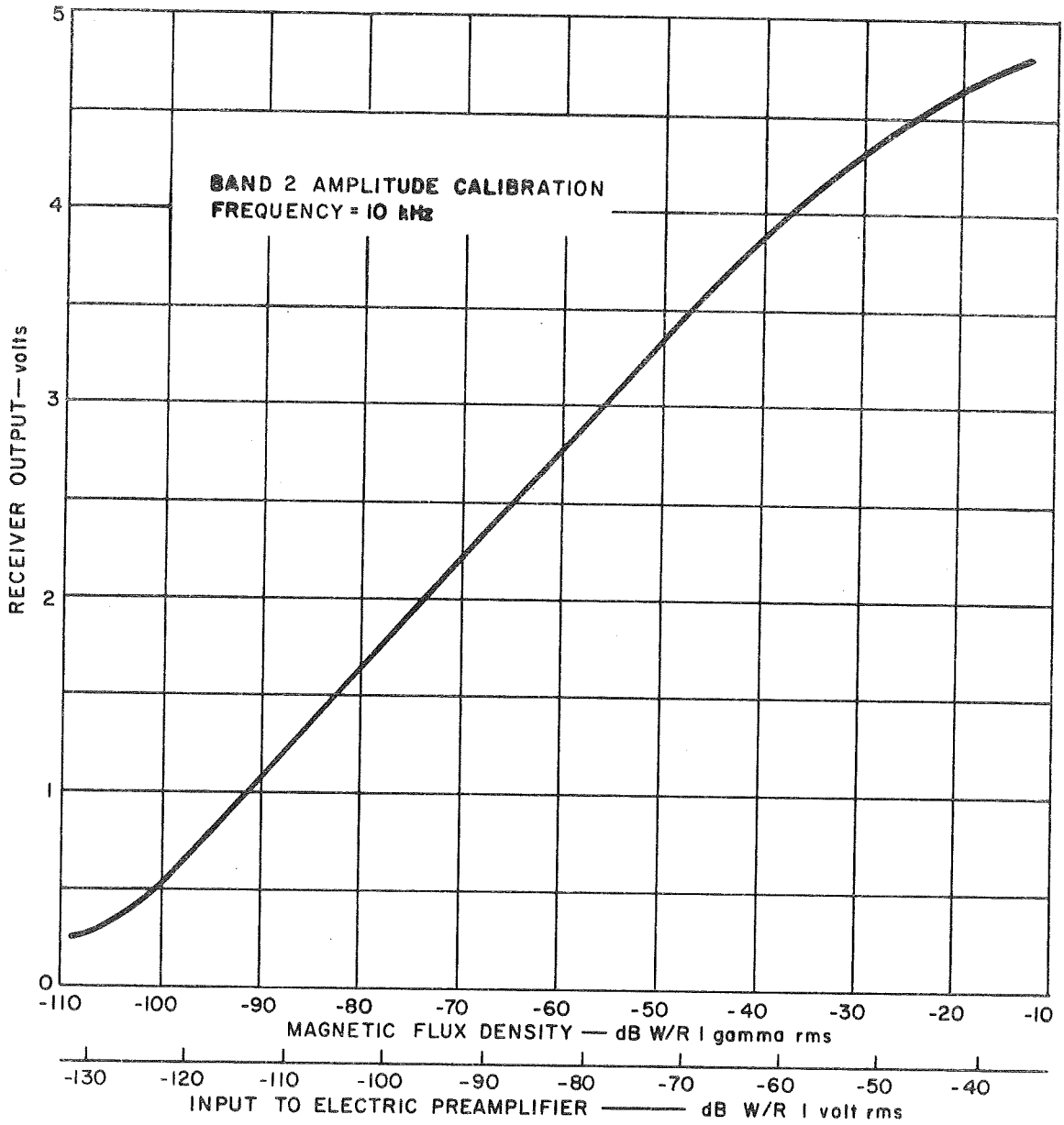

Figure 33. OGO-3 calibration of Band-2 receiver at 10 kHz. Use Figure 31 for calibration at other frequencies. Note the logarithmic response due to the log compressors of Figure 24.

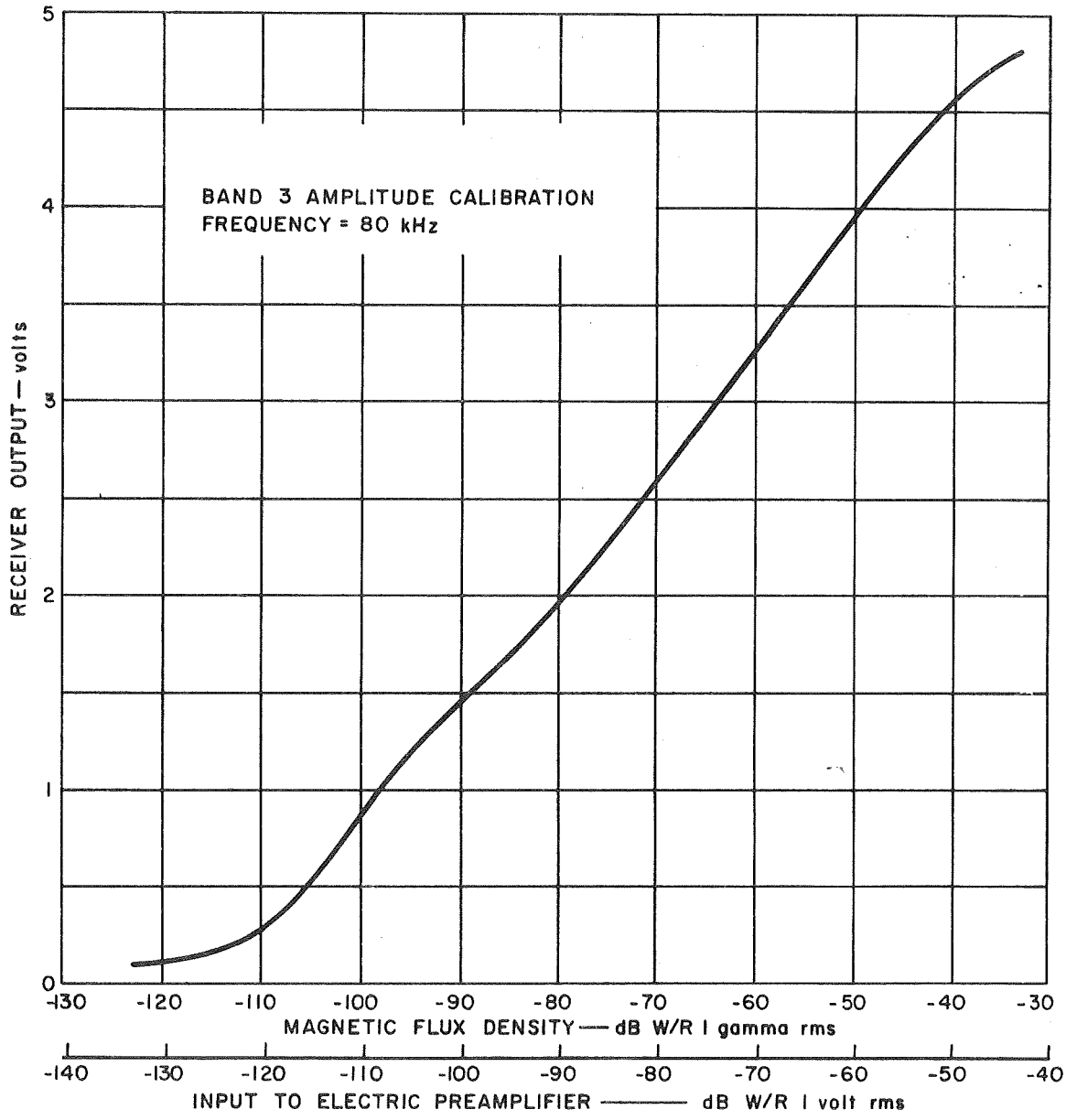

Figure 34. OGO-3 calibration of Band-3 receiver at 80 kHz. Use Figure 31 for calibration at other frequencies. Note the logarithmic response due to the log compressors of Figure 24.

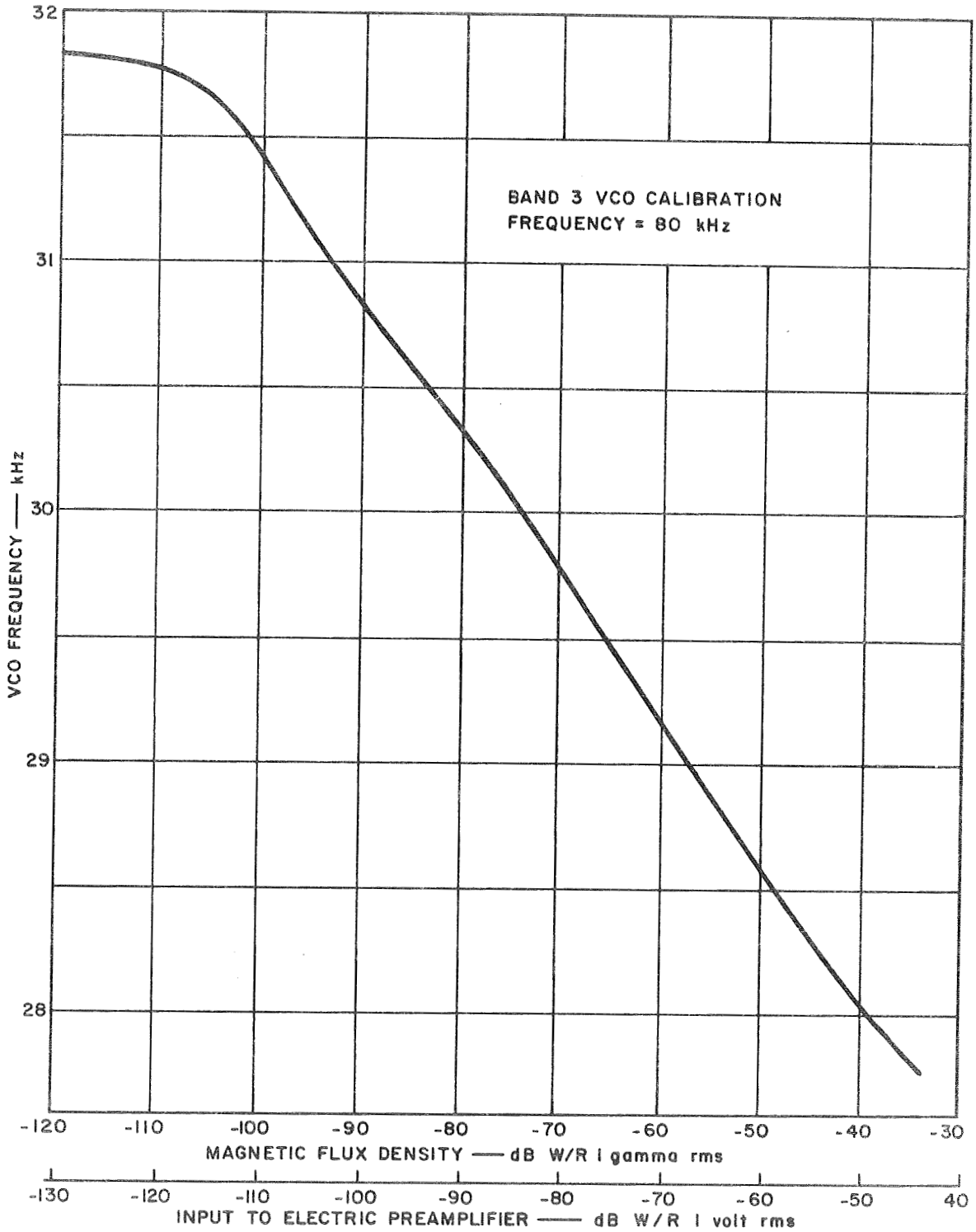

Figure 35. OGO-3 calibration of voltage-controlled oscillator (VCO) for Band 3 tuned to 80 kHz (mode 3). Use Figure 31 for calibration at other frequencies.

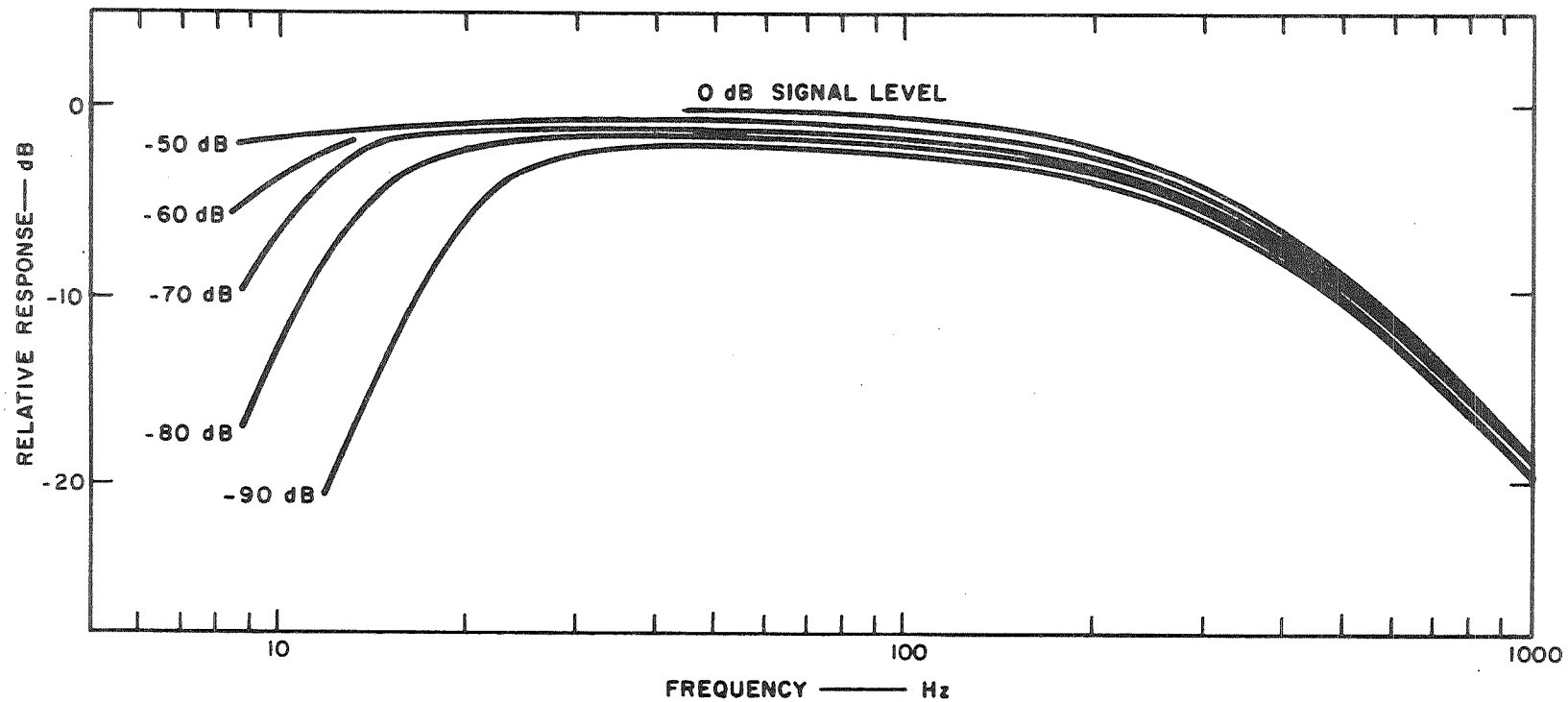

Figure 36. Relative frequency response of ELF broadband receiver ("15-300 Hz") of OGO 3 (modes 1 or 2).

PUBLICATIONS ACKNOWLEDGING NAS 5-2131

Angerami, J. J., Whistler duct properties deduced from VLF observations made with the OGO-3 satellite near the magnetic equator, (submitted to J. Geophys. Res., 1969).

Burtis, W. J., Magnetic radiation observed by the OGO-1 and OGO-3 broad-band VLF receivers, SEL-69-019, Radioscience Lab., Stanford Electronics Labs., Stanford University, Stanford, Calif., August 1969, Eng. Thesis.

Burtis, W. J. and R. A. Helliwell, Banded chorus--a new type of VLF radiation observed in the magnetosphere by OGO 1 and OGO 3, J. Geophys. Res., 74, 3002, 1969.

Carpenter, D. L., C. G. Park, H. A. Taylor, Jr., and H. C. Brinton, Multi-experiment detection of the plasmapause from EOGO satellites and Antarctic ground stations, J. Geophys. Res., 74, 1837, 1969.

Dunckel, N. and R. A. Helliwell, Whistler-mode emissions on the OGO 1 satellite, J. Geophys. Res., 74, 6371, 1969.

Dunckel, N., B. Ficklin, L. Rorden and R. A. Helliwell, Low-frequency noise observed in the distant magnetosphere with OGO 1, J. Geophys. Res., (in press) 1970.

Ficklin, B. P., W. E. Blair, J. H. Wensley, M. E. Mills, N. D. Schlosser and W. H. Zwisler, OGO-1 VLF experiment digital data processing system, Final Rept., Stanford Research Institute, Menlo Park, Calif., April 1967a.

Ficklin, B. P., R. H. Stehle, C. Barnes and M. E. Mills, The instrumentation for the Stanford University/Stanford Research Institute VLF experiment (B-17) on the OGO-3 satellite, Supplemental Rept., Stanford Research Institute, Menlo Park, Calif., May 1967b.

Heyborne, R. L., Observations of whistler mode signals in the OGO satellites, from VLF ground station transmitters, SEL-66-094, Radioscience Lab., Stanford Electronics Labs., Stanford University, Stanford, Calif., Nov. 1966, PhD Dissertation.

Rorden, L. H., L. E. Orsak, B. P. Ficklin and R. H. Stehle, Instruments for the Stanford University/Stanford Research Institute VLF experiment (4917) on the EOGO satellite, Instrument Rept., Stanford Research Institute, Menlo Park, Calif., May 1966.

Smith, R. L. and J. J. Angerami, Magnetospheric properties deduced from OGO-1 observations of ducted and nonducted whistlers, J. Geophys. Res., 73, 1, 1968.

Thorne, R. M., Unducted whistler evidence for a secondary peak in the electron energy spectrum near 10 kev, J. Geophys. Res., 73, 4895, 1968.

GENERAL REFERENCES

IG Bulletin OGO 1, First U. S. Orbiting Geophysical Observatory, Trans. AGU, 46, 326, 1965.

Ludwig, G. H., The orbiting geophysical observatories, NASA Tech. Note, TN D-2646, March 1965.